Selective Electroless Metallization of Patterned Polymeric Films for Lithography Applications

Daniel Zabetakis and Walter J. Dressick*

U.S. Naval Research Laboratory, Center for Bio/Molecular Science & Engineering (Code 6910), 4555 Overlook Avenue, S.W. Washington, D.C. 20375

ABSTRACT The fabrication of electrical interconnects to provide power for and communication with computers as their component complementary metal oxide semiconductor (CMOS) devices continue to shrink in size presents significant materials and processing compatibility challenges. We describe here our efforts to address these challenges using top-surface imaging and hybrid photoresist/self-assembled monolayer patterning approaches, in conjunction with selective electroless metal deposition, to develop processes capable of fabricating appropriate submicron and nanoscale metal features useful as electrical interconnects, as well as plasma-etch-resistant masks and metal diffusion barriers. Our efforts focus on the development of cost-effective methods compatible with a manufacturing environment that satisfy materials and process constraints associated with CMOS device production. We demonstrate the fabrication of ~50-nm-width features in metal with high fidelity and sufficient control of edge acuity to satisfy current industry design rules using our processes and discuss the challenges and opportunities for fabrication of analogous sub-10-nm metal features.

KEYWORDS: electroless • self-assembled monolayer • lithography • pattern • metallization

Downloaded by 194.44.31.30 on November 3, 2009 | http://pubs.acs.org
Publication Date (Web): January 12, 2009 | doi: 10.1021/am800121d

I. INTRODUCTION

Nanotechnology is concerned with the development of materials and procedures required for fabrication, ultimately in an atom-by-atom fashion, of structures and assemblies having unique properties or capabilities dictated by their size, composition, and organization (1−4). However, in many cases, the ability to utilize such precisely structured systems successfully will also require an interface to the macroscopic world. For example, future computers having components of a few nanometers or even molecular dimensions, whatever their ultimate architectures (5−8), will still require some means of power and communication with the user (9). Although metal interconnects provide these functions in current devices, problems such as metal electromigration (10), corrosion (11), and diffusion (12) are expected to compound as metal feature sizes continue to shrink. These issues may ultimately limit the ability of metal features to function as useful electrical interconnects as the active components (e.g., transistors) of devices approach molecular dimensions (i.e., <1 nm) (9). Nevertheless, metal interconnects will still be required to interface users with whatever alternative interconnect technology is adopted as devices approach such ultrasmall dimensions. Conventional nanolithography and metallization techniques, spanning the size range <10−100 nm, offer one possibility for the fabrication of requisite interconnects, provided that the appropriate manufacturing issues can be addressed.

Specifically, any such process suitable for manufacture must satisfy certain basic criteria (13). First, the process must be compatible to the greatest possible extent with standard lithographic fabrication techniques to take full advantage of the available electronics infrastructure. Given the massive financial investments involved, manufacturers are not yet ready or willing to completely abandon existing infrastructure and technologies, even as they move beyond devices with nominal minimal dimensions of 45 nm currently in production (14). Consequently, chances are diminished for the adoption of processes incompatible with current infrastructure and criteria specified by the semiconductor industry roadmap (14) unless their use will provide clear and substantial product performance advantages (e.g., cost, power, speed) that justify the implementation costs.

Second, a process must utilize reliable, cost-effective materials having acceptable properties in each process step. For example, fast-photospeed polymers or photoresists provide ideal materials for pattern definition in the imaging layer at low cost and are highly preferred (15, 16). Metals such as Cu or Al are preferred for interconnects (17) because of their superior electrical conductivities compared to other materials, such as organic conducting polymers. Other metals, such as Ni, are also useful as diffusion barriers (18) for Cu circuitry, as well as plasma etch masks (19) during pattern transfer into the underlying substrate because of their excellent resistance toward degradation under plasma-etching conditions.

Third, deposition of materials onto the substrate during the fabrication process must be selective and additive in nature. Specifically, materials should be strongly adhered to the substrate *only* where desired without the need for

* To whom correspondence should be addressed. E-mail: walter.dressick@nrl.navy.mil.

Received for review October 14, 2008 and accepted November 26, 2008

DOI: 10.1021/am800121d

This article not subject to U.S. Copyright. Published 2009 by the American Chemical Society

Published on Web 01/12/2009

Downloaded by 194.44.31.30 on November 3, 2009 | http://pubs.acs.org
Publication Date (Web): January 12, 2009 | doi: 10.1021/am800121d

additional process steps to remove any loosely bound or spurious "waste" deposits elsewhere. Material deposition process steps should also ideally be aqueous-based to mitigate health and environmental concerns and rapid (<2 min) to maximize process throughput and minimize cost.

We are investigating various molecular self-assembly processes, in conjunction with electroless (EL) metal deposition (20−27) and ultraviolet (UV) (19, 28−48), X-ray (31, 49−52), proximal probe (23, 53−58), microcontact printing (μCP) (31, 59−61), ion beam (49, 62), or electron beam (22, 23, 29, 30, 35, 63) patterning techniques, with the goal of developing processes suitable for the manufacture of nanoscale metal features useful as plasma etch masks, diffusion barriers, and electrical interconnects for electronics applications. In this Spotlight on Applications paper, we describe our work and some related work by others toward this goal. The Appendix at the end of this paper defines the various acronyms and trade names used throughout the text. We begin with a description of current EL processes for patterned metal deposition and the development of new Sn-free EL catalysts required for the selective EL plating of nanoscale features with proper control of feature critical dimensions for electronics applications. There follow descriptions of approaches based on the use of these catalysts for the selective metallization of (1) top-surface imaged self-assembled monolayers (SAMs) or thin polymer films and (2) patterned composite polymer photoresist−SAM films. We restrict our discussion to organosiloxane-based SAMs (64), given the importance of Si as an electronics substrate. In many cases, however, the general photochemical and EL concepts underlying our imaging and metallization approaches, respectively, will be readily transferable to other electronically interesting SAM−substrate systems (65, 66), such as organothiol- (67), organophosphonate- (68), or aryl- (69) SAM-GaAs. Finally, the fabrication of sub-10-nm metal features with high fidelity and acceptable control of feature critical dimensions (i.e., ≤5% variation in feature dimensions) for use as electrical interconnects, plasma etch masks, or diffusion barriers will certainly require the development of even more advanced systems than those reported here. Therefore, we conclude this paper with an account of some advances concerning related new Sn-free and Pd-free EL catalysts and selective metallization approaches suitable for manufacture and their use with patterned polymer and SAM template films.

II. EL METAL DEPOSITION

EL deposition is a process for chemical deposition of metal from a solution containing a reducing agent and a complex of an ion of the metal to be plated onto a catalyzed substrate surface (70). The process is generally inexpensive and can be performed in a manufacturing environment at or near room temperature under ambient, aqueous conditions. EL plating is amenable for the deposition of conformal metal films onto either planar (19) or nonplanar (21, 22, 71) substrates, including properly catalyzed (vide infra) insulators. Metals useful for electronics applications that can be readily plated include noble metals (e.g., Au, Ag, Pt, and Pd) and certain other first-row transition metals such as Cu, Ni, Co, and Fe (72, 73) and their alloys. Recently, the EL deposition of Al has also been demonstrated using an ionic liquid solvent (74). Many of these metals are themselves autocatalytic and will sustain further EL metal deposition even after the surface catalyst is covered by the metal deposit.

EL deposition is an exceedingly complex process involving multiple simultaneous redox processes at or near a substrate surface that is continually changing its composition, structure, and morphology as the plating process proceeds. Despite various experiment-based models (75−79), mechanistic details of metal deposition at the substrate surface remain unclear. Mixed potential theory (MPT) (80) remains perhaps the most widely used model for EL deposition. It describes EL plating in terms of an initial spontaneous oxidation of the reductant at a catalytic surface, leading to electron charging of the surface until its electrochemical potential becomes sufficiently negative to reduce the metal complex to metal. MPT provides an adequate description of the plating process when electron transfer between the reductant and metal ion is mediated by the catalytic surface and can be described by diffusion-controlled or electrochemically controlled partial reaction currents (80−82). It fails if direct electron transfer between the reductant and metal ion (83) can also occur. More recent ab initio molecular orbital studies by Homma and co-workers (84−88) suggest that the stability of five-coordinate intermediates formed by the attack of hydroxide on reductants adsorbed on the surface, together with the electron acceptor ability of the surface, comprises key mechanistic steps for the EL plating process. As a result of advances such as these, improved EL deposition models that further our understanding of the process continue to be developed (89−91).

II-A. EL Pd−Sn Catalysts. Commercial EL catalysts are typically core−shell Pd−Sn colloidal species exhibiting complex compositions and chemistries (92−94). The core comprises a Pd-rich, zerovalent, crystalline Pd−Sn alloy (Pd_xSn_{1-x}; $0.6 < x < 1.0$) (92, 95), which functions as the catalytically active component for EL deposition. It is surrounded by a β-stannic shell consisting primarily of μ-hydroxy-bridged Sn^{II} and Sn^{IV} oligomers (92, 96) whose chemical composition and thickness can vary profoundly with the pH, solution composition, temperature, oxygen exposure, and catalyst age and processing history (97−99). Consequently, although catalyst particles are typically ∼2 nm in diameter (92, 100), size ranges from 1 to ∼5 nm have been reported (97−99, 101). The β-stannic shell stabilizes the catalyst dispersion in aqueous solution against aggregation by virtue of its inherent negative charge and hydrogen-bonding interactions with associated water molecules (93). In addition, Sn^{II} species within the shell reduce any Pd^{II} formed via inadvertent oxidation of the Pd−Sn core (e.g., due to oxygen exposure) (92), maintaining the zerovalent Pd−Sn core state required to catalyze EL deposition. Finally,

Downloaded by 194.44.31.30 on November 3, 2009 | http://pubs.acs.org
Publication Date (Web): January 12, 2009 | doi: 10.1021/am800121d

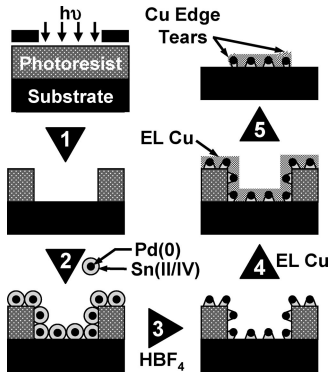

FIGURE 1. Subtractive EL metallization. The process sequence is shown for patterned metallization based on EL metal deposition onto a Pd–Sn-catalyzed patterned photoresist, followed by lift-off of the excess photoresist and unwanted EL metal.

the β-stannic shell also adheres the catalyst particle to the substrate to be plated (92, 96).

The adhesive properties of the β-stannic shell are critically important for use of the Pd–Sn colloid as an EL catalyst. The β-stannic shell does not adhere well to clean, hydroxylated inorganic oxide surfaces like those of native silicon oxide, unlike other simpler monomeric tin(IV) alkoxides (102, 103) or tin(II) salts (104, 105) that chemisorb directly to various hydroxylated surfaces. In contrast, the β-stannic shell does adhere to many other surfaces, including polymer photoresists, useful for electronics applications. However, adhesion is generally weak, suggesting that binding occurs via van der Waals or other noncovalent interactions.

A subtractive process, as illustrated in Figure 1, is typically employed for patterned metallization using Pd–Sn catalysts because of their poor binding selectivity characteristics. A photoresist coating the substrates is first imaged and developed (step 1) to define the desired pattern. The Pd–Sn colloid is then adsorbed onto both the photoresist polymer and the areas of the substrate uncovered on the channel floors defined by the developed photoresist (step 2). Before EL metallization can proceed, however, an acid "acceleration" treatment that dissolves a portion of the β-stannic shell to expose the catalytically active Pd–Sn core to the EL plating solution (step 3) is usually performed. Treatment temperature, time, and acid concentrations are carefully controlled to prevent pattern degradation via dissolution of that portion of the β-stannic shell anchoring the catalyst particle to the substrate. The substrate is then immersed in the EL plating bath, which deposits metal over the entire catalyzed surface (step 4). Metal growth usually continues in an autocatalytic fashion even after the Pd–Sn is fully coated. Selectivity is achieved through dissolution of the remaining photoresist following plating, which lifts off the metallized photoresist from the metal patterned substrate (step 5).

There are several disadvantages to subtractive EL metal deposition as practiced in Figure 1. Because the Pd–Sn catalyst adsorbs nonselectively to both photoresist and substrate, metal deposition occurs everywhere in a subtractive process. Disposal of the waste photoresist and unwanted metal adds to the process cost and can pose environmental hazards. During the lift-off process, tearing of the metal at the photoresist–substrate boundary at the channel edge increasingly compromises the edge acuity of the desired metal feature remaining on the substrate as the feature size decreases. In addition, undesirable metal lift-off from the substrate can also occur, especially on smooth substrates for thicker metal features required for use as electrical interconnects, because of the weak adhesion of the Pd–Sn catalyst.

Efforts to surmount these problems have focused primarily on the development of alternative schemes that directly deposit a pattern of the Pd–Sn catalyst "ink" onto the surface for plating. For example, μCP provides an efficient means for additive EL plating via selective deposition of catalyst solely onto those regions of the surface to be plated (106, 107). In this method, a surface-modified poly(dimethylsiloxane) stamp bearing patterned features in relief is treated with Pd–Sn colloid "ink" and the stamp is used to transfer the colloid pattern directly onto the substrate, which is then plated. Although unable to directly catalyze EL deposition, tin(II) salt or colloid inks (108) are also effective. In this case, reduction of a transition metal ion such as Ag^{I} to an active EL catalyst such as Ag^{0} by the Sn^{II} surface pattern is required to initiate EL plating. Because feature resolution for μCP is improved for smoother substrate surfaces (66, 109), metal adhesion issues remain a concern. Nevertheless, through the use of chemisorbed (protonated) (aminoalkyl-)siloxane SAMs capable of electrostatically interacting with the anionic Pd–Sn catalyst (92, 110), adhesive microscale EL Ni features of thickness ~400 nm have been fabricated via μCP on smooth glass plates (107). The fabrication of submicron and eventually nanoscale EL metal features will clearly depend on the development of improved catalysts (106) and μCP techniques and equipment capable of printing sub-100-nm resolution features (111, 112).

Metal adhesion can also be improved by using substrates having naturally, or mechanically/chemically induced, roughened surfaces that mechanically stabilize the EL plate. For example, inkjet printing provides an efficient means to directly write patterns of Pd–Sn on paper (20). The Pd–Sn colloid binds well to the cellulose fibers (72, 113) comprising paper and maintains its ability to catalyze EL metal deposition. EL plating of Pd–Sn-patterned paper provides a composite material of use for decorative, flexible electronics, and microwave applications. For example, Figure 2 illustrates an array of EL Cu hexagonal split-ring resonators useful for high-performance microwave applications prepared in this fashion. Although the Cu feature width is limited to ~100 μm because of geometric restrictions on the minimum printable Pd–Sn droplet size and the natural roughness of the cellulose fibers (diameter ~20 μm), the latter enhances adhesion of the Cu deposit. In fact, surface microroughening enables the use of Pd–Sn colloid-based EL deposition processes for fabrication of printed circuit boards, filling via holes, and numerous other lower-resolution electronics applications (114, 115). However, for submicron or smaller feature sizes, the surface roughness increasingly limits feature definition during patterning and ultimately compromises the fidelity

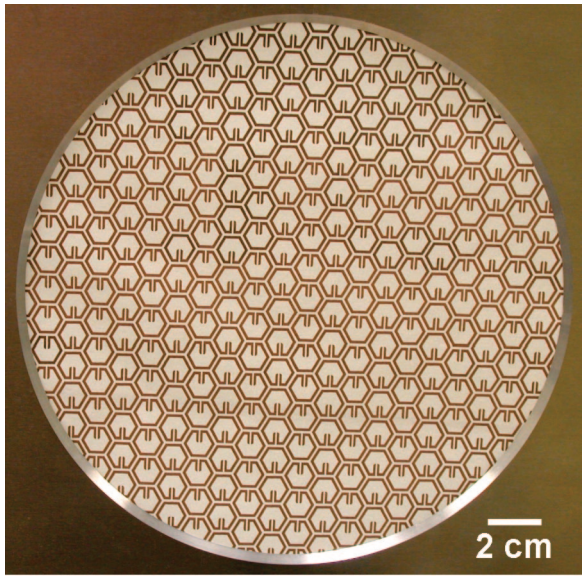

FIGURE 2. EL Cu microwave split-ring resonators on paper. Process sequence: (1) inkjet print Pd−Sn catalyst pattern on paper; (2) paper conditioning and acceleration in 0.1 M HCl(aq) (3 min); (3) Fidelity 1025 EL Cu bath (40 °C, 12 min) treatment; (4) H_2O rinse; (5) vacuum drying (15 min, 80 °C, ~28 in. Hg).

of the plated metal feature. Consequently, alternative methods are required to control EL metal adhesion at these dimensions.

II-B. Sn-Free EL Pd Catalysts. The use of covalent, rather than noncovalent, interactions to adhere the catalytic Pd core to the surface to be plated represents a straightforward and attractive means to enhance EL metal adhesion (42, 45, 46). In addition to increased adhesion strength, the specificity of covalent interactions offers a means to improve the selectivity of the EL plating process (44). Our approach involves a partitioning of the catalytic and adhesive functions of the Pd−Sn colloid between the particle and the substrate surface, respectively, that simplifies the nature of the catalyst particles. Because specific, covalent interactions between ligand functional groups present at a substrate surface and catalytic Pd species anchor the catalyst, the adhesive β-stannic shell is no longer required.

There are several advantages to using such an approach. First, it simplifies the composition of the catalysts and eliminates the use of environmentally hazardous Sn species in the process. Furthermore, the use of surface ligand-binding sites increases the versatility of the process, eliminating Pd−Sn catalyst stability issues by allowing the use of air-stable Pd^{II} species that can be reduced in situ during the plating process to active Pd^0 catalysts. In addition, the nature of the ligands provides a means to tune the binding strength (42, 45, 46), with chelating and/or good π-acceptor ligands capable of stabilizing the bond to the catalytically active Pd^0 state via π-back-bonding interactions preferred.

Although some substances naturally possess ligand functional groups as an integral part of their structure (116−118), most polymers and materials useful as electronics substrates do not. Consequently, ligand functional groups must first be created on their surfaces to enable catalysis via our Sn-free Pd method. Scheme 1 illustrates the structures of several

Scheme 1. Some Ligand Organosilanes and Their SAM Chemisorption Reactions

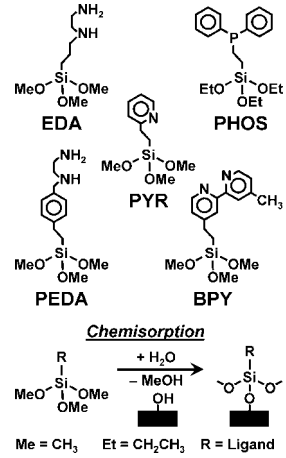

organosiloxane ligands capable of efficiently covalently binding Pd species for EL plating. Organosiloxane ligands provide a convenient means to introduce the requisite surface ligands onto the substrate to be plated as SAMs (64, 119, 120) via straightforward chemisorption reactions with reactive substrate hydroxyl groups. Such groups may occur naturally on the substrate surface (e.g., native silicon oxide) (19, 64, 119, 120) or may be created via mild chemical or radio-frequency (RF) plasma treatment (e.g., diamond (36) or polymers (121)).

Although binding of monomeric Pd^{II} species to surface ligand sites on SAMs readily occurs, the discrete monomeric Pd^{II}/ligand complexes formed do not support EL metal deposition (122−124). Because the bound Pd species are typically present at concentrations of only $\sim(2-4) \times 10^{14}$ Pd atoms · cm^{-2} (27), the sizes and numbers of Pd^0 islands formed during reduction are insufficient to offset quenching of the metallization process by oxygen and inhibitors present in the EL bath (125). In addition, the reactivity of smaller Pd^0 islands is also diminished by their interaction with the ligand, which can reduce the density of states near the Fermi level that maintain the metallic properties of the particle required for catalysis (124). Consequently, EL metal deposition, even if it initiates on such surfaces, cannot be sustained.

Previous work using Pd−Sn colloids has shown that sustained EL metallization requires a threshold surface concentration of $>10^{15}$ Pd atoms · cm^{-2} (126), a value that exceeds levels for monomeric Pd^{II}/ligand SAM complexes. Consequently, metallization processes using simple ligand SAMs, such as those shown in Scheme 1, will require binding of Pd-based oligomers or colloids to exceed the threshold. Fortunately, oligomers and colloids capable of covalently binding ligand SAMs are readily formed by controlled hydrolysis or the reduction of aqueous Pd^{II} solutions. For example, hydrolysis of $PdCl_4^{2-}$ in aqueous solution proceeds at pH > 1 via sequential reversible loss of chloride ligands to form mixed choro−aquo complexes (e.g., eqs 1 and 2).

Downloaded by 194.44.31.30 on November 3, 2009 | http://pubs.acs.org
Publication Date (Web): January 12, 2009 | doi: 10.1021/am800121d

Downloaded by 194.44.31.30 on November 3, 2009 | http://pubs.acs.org
Publication Date (Web): January 12, 2009 | doi: 10.1021/am800121d

$$PdCl_4^{2-} + H_2O \leftrightarrow PdCl_3(H_2O)^- + Cl^- \quad (1)$$

$$PdCl_3(H_2O)^- + H_2O \leftrightarrow PdCl_2(H_2O)_2 + Cl^- \quad (2)$$

As the solution pH is increased, deprotonation of the coordinated water molecules increasingly occurs to generate mixed chloro−aquo−hydroxy species (e.g., eq 3).

$$PdCl_2(H_2O)_2 \leftrightarrow PdCl_2(H_2O)(OH)^- + H^+ \quad (3)$$

Subsequent condensation of these species (e.g., via eq 4) generates μ-hydroxy- and/or μ-chloro-bridged oligomers whose length and composition depend on the preparation conditions, including the solution pH, chloride levels, and temperature (24, 25, 27).

$$3PdCl_2(H_2O)(OH)^- \rightarrow Cl_2Pd(\mu\text{-}OH)_2Pd(\mu\text{-}OH)(\mu\text{-}Cl)PdCl(H_2O)^- + 2Cl^- + 2H_2O \quad (4)$$

For example, recent EXAFS studies (127) have confirmed the presence of oligomers containing 3−9 Pd^{II} sites with structures similar to those shown in eq 4 for palladium(II) salts hydrolyzed in room temperature 0.6 mol/kg NaCl(aq) at pH 4−6. Self-assembly of the oligomers formed via eq 4 generates colloidal particles having labile surface sites capable of covalently binding surface ligands as effective EL catalysts (25).

The ability to control the size and polydispersity of such colloidal particles is critically important for their use as EL catalysts for selective plating, especially for nanoscale features. As illustrated in Figure 3A, the size of a colloid particle can comprise a significant fraction of the nanoscale feature size. EL metallization is an isotropic process, so that larger catalyst particles will naturally yield larger metal particles during plating (26). Therefore, if catalyst particles having sizes comparable to the feature are bound, the resulting EL metal film may fail to properly replicate the dimensions of the feature pattern (45). This loss of pattern fidelity will be accompanied by degradation of the plated feature edge acuity when large colloid particles bind at the edge of the pattern. In addition, under such circumstances, undesirable metal bridging between adjacent feature patterns can also occur for closely spaced features, compromising the pattern fidelity, as shown in Figure 3A.

Consequently, because the largest sized colloids present in the dispersion will influence metal feature resolution, the ideal catalyst comprises a monodisperse colloid having particles of the smallest size possible. Unfortunately, no colloid is truly monodisperse. In practice, we have empirically observed that the largest catalyst particles in a colloidal dispersion should be no more than ∼10% the size of the ligand SAM pattern to yield EL plated features satisfying the current 5% design rule limiting feature size variations for electronics applications (23, 29−31, 63). However, exceptions do exist. For example, colloid particle binding is also dependent upon the nature (21) and coverage (26) of the ligand on the surface to be plated. In fact, smaller components of colloidal dispersions are preferentially bound at surfaces bearing depleted ligand levels (26), permitting selective EL plating of features smaller than would normally be expected using polydisperse colloids of a given average particle size and particle size range (24, 45).

These behaviors suggest that a repertoire of Pd-based colloids is desirable to address the various circumstances likely to be encountered during selective EL plating of feature patterns. The average colloid particle size and polydispersity are readily tuned via control of the Pd^{II} hydrolysis conditions. For example, hydrolysis of $PdCl_4^{2-}$ in a mildly acidic solution containing added chloride ions occurs relatively slowly (27). The added chloride limits the production of aquo species according to the equilibria of eqs 1 and 2, while the presence of acid minimizes their dissociation via equilibria such as eq 3. As a result, the generation of $PdCl_2(H_2O)(OH)^-$ and related species capable of nucleating oligomers via eq 4 occurs simultaneously with the growth of existing oligomers. Under these circumstances, highly polydisperse colloids having both large average particle size and particle size range are formed. Once formed, the colloidal particles will continue to grow, as long as sufficient $PdCl_2(H_2O)(OH)^-$ is present, until size-induced aggregation leading to their separation from the liquid phase as a bulk precipitate occurs. Therefore, the colloid, once formed, must be stabilized by the addition of excess chloride to suppress the equilibria of eqs 1−3 leading to the formation of $PdCl_2(H_2O)(OH)^-$.

One such catalyst of this type, referred to as PD1, is easily prepared by the hydrolysis of ∼0.38 mM Na_2PdCl_4 in a 10 mM NaCl(aq) solution at pH ∼5 (25). The pH is maintained during the ∼20 h room temperature hydrolysis using a 0.01 M morpholinoethanesulfonate buffer, which does not interfere with the reactions of eqs 1−4 because it does not coordinate Pd^{II} ions (128). Following completion of the hydrolysis, a straw, yellow Pd^{II} colloidal dispersion is obtained. The dispersion is stabilized by the replacement of 10% of its volume by an equivalent volume of a 1 M NaCl(aq) solution, which raises its chloride level to ∼0.11 M and provides a catalyst stable for ∼4−6 weeks at room temperature. The atomic force microscopy (AFM) examination of the PD1 catalyst in Figure 3B yields an average particle size of ∼30 ± 12 nm and a particle size range of ∼4−53 nm (25), values consistent with the simultaneous nucleation and growth of colloidal particles expected under these hydrolysis conditions.

The formation of smaller colloidal particles requires the enhancement of particle nucleation at the expense of particle growth. Ideally, all of the $PdCl_4^{2-}$ initially present is instantaneously converted into species capable of forming nuclei. Although a large number of nuclei of similar size will form, almost no $PdCl_4^{2-}$ remains to fuel their growth via eqs 1−3. Under such conditions, a large number of monodisperse colloidal particles of very small size would be formed. In practice, however, nuclei formation in this manner is not an instantaneous process so that a colloid having low polydispersity is actually formed.

There are several methods applicable for the preparation of such smaller near-monodisperse colloids, including pH-jump, chemical reduction, and temperature-jump approaches. Although we have not utilized temperature-jump methods,

we have successfully prepared colloidal particles using both pH-jump (24) and chemical reduction (23, 29, 63) approaches. In the pH-jump approach, the pH of a strongly acidic solution containing $PdCl_4^{2-}$ is quickly raised to pH >7 by the addition of an aliquot of base (24). This leads to rapid formation via the equilibria of eqs 1−3 of large amounts of $PdCl_2(H_2O)(OH)^-$ required for particle nucleation and at the same time depletes the levels of $PdCl_4^{2-}$ required for subsequent particle growth. After a few hours, the dispersion is brought to pH ∼3 by the addition of HCl(aq) and chloride levels are raised to ∼0.25 M by the addition of NaCl(aq) to arrest colloid development.

PD2 (24), a catalyst prepared in this manner, exhibits an average colloid particle size of 9 ± 3 nm and a particle size range of ∼4−18 nm, as shown in the AFM image of Figure 3C. PD2 is a much more reactive colloid than PD1, in part because of its smaller size, composition differences, and highly reactive surface sites, and exhibits a useful lifetime of only ∼1 day at room temperature. However, its properties are entirely consistent with those expected for colloidal species formed under conditions in which nucleation dominates particle growth.

Because chemical reduction can occur quite rapidly, even smaller Pd-based colloids can be formed. Colloid formation is initiated via the direct chemical reduction of Pd^{II} to Pd^0 in the presence of a soluble stabilizing ligand rather than via the hydrolysis reactions of eqs 1−4. The free Pd^0 atoms generated during reduction self-assemble to form colloids. The colloid size and stability are governed by the choice of the stabilizing ligand and reductant. We have chosen poor π-acceptor ligands, such as citrate, which are expected to bind weakly to the Pd^0 sites on the colloid surface as stabilizers. Although such weak stabilizer ligands limit the colloid lifetime to a few days, their displacement at ligand SAMs bearing pyridines (23, 29, 44, 63), phosphines (35, 43, 129), or other strong π-acceptor ligands (42) capable of strong π-back-bonding with zerovalent metal sites facilitates covalent bonding of the colloid to the substrate to be plated. For example, Figure 3D shows a TEM of PD0 (29, 63), a catalyst prepared by the reduction of a palladium(II) citrate complex using tetrakis(hydroxymethyl)phosphonium chloride. The average particle size of PD0 is ∼2.6 ± 0.8 nm, with a particle size range of just ∼1−5 nm, values consistent with the more rapid nucleation expected for a chemical reduction process than the pH-jump method.

III. SELECTIVE EL PLATING VIA TOP-SURFACE IMAGING (TSI) APPROACHES

The effective use of catalysts such as PD1, PD2, or PD0 for selective metallization requires the development of efficient ligand-based surface patterning techniques. Conventional patterning methods rely on the patterned exposure of thin (∼1 μm thickness) photoresist films using UV, X-ray, or e-beam sources (13). Chemical changes induced at low exposure doses (e.g., typically <10 mJ · cm^{-2} for UV exposures) in the photoresist greatly increase or decrease its solubility in a subsequent solution-based development step, leading to a 3D structured film that replicates (i.e., positive-tone) or complements (i.e., negative tone), respectively, the mask pattern in the photoresist at the substrate surface. The remaining patterned photoresist protects the underlying substrate during the subsequent plasma reactive ion etch (RIE) that transfers the pattern into the substrate during integrated circuit fabrication.

The highest resolution feature (R) that can be printed in the photoresist (13, 14) is determined by the numerical aperture (NA) of the optical system used, a geometric factor (k) characteristic of the optical system, and the wavelength of light (λ) used for exposure according to eq 5.

$$R = k\lambda/\mathrm{NA} \tag{5}$$

The fidelity with which the feature is printed is determined primarily by the depth of focus, D, which describes the ability to focus the pattern image through the entire thickness of the photoresist. D is again a function of NA, λ, and another optical instrument factor (k'), as shown in eq 6.

$$D = \pm k'\lambda/\mathrm{NA}^2 \tag{6}$$

Because further improvements in k, k', and NA are increasingly limited by physical and technological constraints (14), the ability to print ever smaller (i.e., higher-resolution) features requires the use of shorter λ (i.e., more energetic) light. Unfortunately, as λ decreases with the use of deeper UV light, a point is reached where (1) the fidelity is compromised because a clear image can no longer be maintained through the entire thickness of the photoresist and/or (2) the photoresist absorbance increases such that light can no longer fully penetrate the photoresist film. In either case, the patterning process is compromised.

TSI is an EL-compatible process that addresses these problems by partitioning the imaging and plasma-etch-resistance functions of the typical photoresist between a photosensitive polymer film and refractory oxide or metal film, respectively (130−134). Imaging is accomplished via exposure of only the outermost molecular layer(s) of a photosensitive polymer film, avoiding the depth-of-focus and transparency issues associated with conventional photoresists. The new chemical functional groups generated on the exposed polymer surface provide convenient sites for selective grafting or adsorption of refractory oxides (135, 136), metals (137, 138), or their precursors capable of withstanding the plasma etch process. For example, the reaction of $SiCl_4$ with surface hydroxyl groups generated on or in the outermost regions of the exposed polymer surface generates SiO_2, which possesses the requisite plasma-etch resistance for the pattern transfer process, during the RIE step (133).

III-A. TSI and Pd−Sn EL Processes. We have adapted the TSI process for fabrication of patterned EL metal films useful as plasma-etch-resistant masks or electrical interconnects by using organosiloxane SAMs as ultrathin imaging layers for pattern definition (42, 44, 45). In our initial work, we have demonstrated the feasibility of the approach using simple nonligand phenylsiloxane SAMs patterned with deep-UV light at 193 nm in conjunction with conventional Pd−Sn catalyst-based EL plating (139−142) according to Figure 4A. Mass spectroscopy and electron spectroscopy for chemical analysis experiments confirm the

Downloaded by 194.44.31.30 on November 3, 2009 | http://pubs.acs.org
Publication Date (Web): January 12, 2009 | doi: 10.1021/am800121d

Downloaded by 194.44.31.30 on November 3, 2009 | http://pubs.acs.org
Publication Date (Web): January 12, 2009 | doi: 10.1021/am800121d

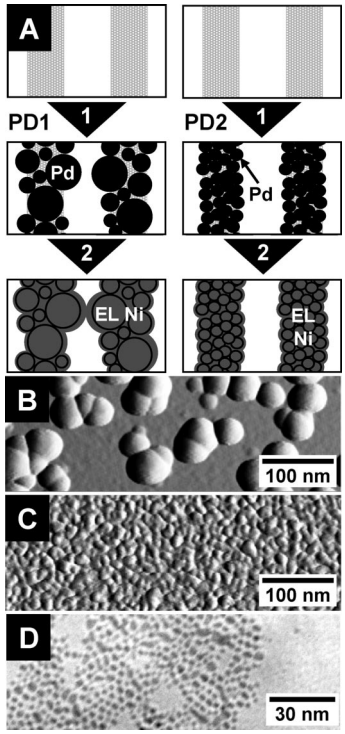

FIGURE 3. Sn-free EL Pd catalysts: (A) effects of the Pd catalyst size and polydispersity on the control of the pattern fidelity and edge acuity during plating of nanoscale features; (B) AFM image of the PD1 catalyst; (C) AFM image of the PD2 catalyst; (D) TEM image of the PD0 catalyst. Parts B and C are reproduced with permission from *J. Electrochem. Soc.*, 1997, *144*, 3425. Copyright 1997 The Electrochemical Society.

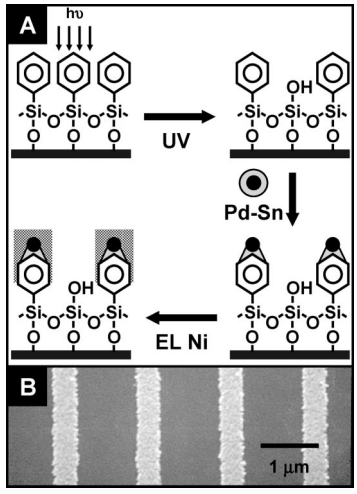

FIGURE 4. Patterned EL metallization using Pd−Sn: (A) UV patterning and EL metallization scheme; (B) Ni lines (light areas) of ∼400-nm width prepared via the scheme of part A.

expulsion of benzene as the sole photoproduct from the SAM during irradiation and the concomitant generation of silanol groups on the surface, respectively, consistent with a simple Si−C bond photocleavage mechanism (45, 47). The exposure dose required to sufficiently clear the organofunctional group from the surface to permit selective Pd−Sn binding and EL plating is a critical process variable because it determines the efficiency and throughput of the entire manufacturing process. A "spectroscopic" exposure dose, which represents the energy required to remove >95% of the phenyl chromophore from the SAM, of ∼400 mJ · cm^{-2} is observed for the phenylsiloxane SAM chemisorbed on a fused-silica substrate. Similar doses are observed for phenethylsiloxanes and related simple aromatic siloxanes, consistent with simple Si−C photocleavage as a general photodecomposition mechanism for these SAMs. However, isolated phenyl (or related aromatic) residues still remain on the surface at this point and can bind sufficient Pd−Sn to catalyze EL metallization. Consequently, "metallization" doses of ∼500−800 mJ · cm^{-2} are often required to clear the fused-silica surface sufficiently to permit reproducible, selective plating using the Pd−Sn catalyst.

It is important to note that for a given SAM the dose also varies with the packing density of the SAM on the surface and the nature of the underlying substrate. This behavior reflects differing abilities of adjacent SAM organofunctional groups and substrates to dissipate the energy absorbed by the SAM. For example, SAMs chemisorbed onto conducting substrates such as native silicon oxide wafers often exhibit exposure doses ∼2−3 times higher than the same SAMs chemisorbed onto insulators such as fused silica (45). In addition, exposure doses of more closely packed SAMs (63) prepared via chemisorption of organofunctional trichlorosilanes (e.g., [*p*-(chloromethyl)phenethyl]trichlorosilane) are often a factor of ∼2 larger than doses for SAMs prepared using corresponding organofunctional dimethylmonochlorosilanes (e.g., [*p*-(chloromethyl)phenethyl]dimethylchlorosilane) (143), whose packing is sterically hindered by the methyl groups bonded to the Si site. These packing- and substrate-dependent exposure doses, together with metal adhesion reliability issues, represent manufacturing problems for the Pd−Sn EL process of Figure 4A. Nevertheless, the method permits deposition of ∼20−40-nm-thick adherent metal features having line widths as small as ∼0.3−0.4 μm on Si wafers, as shown in Figure 4B. The resulting metal features function as efficient plasma-etch-resistant masks during RIE pattern transfer in the fabrication of functional CMOS transistors and capacitors, which exhibit performances and lifetimes comparable to those of traditionally manufactured analogues (139−141).

III-B. Ligand TSI and Sn-Free EL Pd Methods. Analogous EL metal features exhibiting improved adhesion (42, 46) may be fabricated using Sn-free Pd catalysts with ligand SAMs, as shown in Figure 5A. For example, patterned 193-nm exposure of the PYR SAM (Scheme 1) sufficiently damages the N ligating site to support selective EL Ni deposition (44). In this case, the spectroscopic and metallization doses are identically ∼1.5 J · cm^{-2} for a PYR SAM chemisorbed to fused silica (42, 45) (∼4.5 J · cm^{-2} metallization dose on a native silicon oxide wafer) (27, 44), consistent with the selectivity of the Pd^{II} colloid covalent binding process at the surface pyridyl ligand sites. Figure 5B shows an Auger Pd line scan of one such patterned PYR SAM, confirming selective, covalent binding of Pd^{II} sites within the PD1 colloid to the intact PYR ligands remaining on the unirradiated areas of the Si wafer substrate. The corresponding Auger line scan after Ni plating is shown in

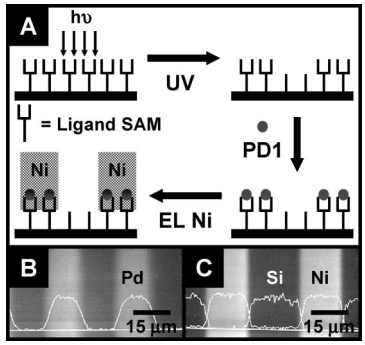

FIGURE 5. Fabrication of positive-tone EL metal features using a TSI ligand approach: (A) General scheme for UV patterning of ligands with selective EL plating; (B) Pd Auger line scan of patterned lines prepared via the scheme of part A after Sn-free Pd catalysis. Reproduced with permission from *J. Electrochem. Soc.*, 1994, *141*, 210. Copyright 1994 The Electrochemical Society); (C) Ni and Si Auger line scans of features from part B after EL Ni plating showing metal deposition selectivity. Reproduced with permission from *ACS Symp. Ser.*, 1994, *537*, 210. Copyright 1994 American Chemical Society).

Figure 5C, which indicates that EL Ni is deposited selectively onto those areas bearing the Pd^{II} colloidal species.

The high 193-nm spectroscopic exposure dose observed for the PYR SAM on fused silica compared to corresponding aromatic siloxanes of similar structure is somewhat misleading, given the identical Si−C photocleavage mechanisms observed for both SAMs (45). Much of the difference can be attributed to the lower extinction coefficient for absorption of 193-nm light by the 2-pyridylethyl chromophore ($\varepsilon_{193} \cong 7-8 \times 10^3$ cm^2 · mol^{-1}) (27) compared to that of a corresponding phenethyl analogue ($\varepsilon_{193} \cong 3 \times 10^4$ cm^2 · mol^{-1}) (45). However, contributions to the increased dose from energy degradation pathways related to known pyridyl *N*-silanol hydrogen bonds (144, 145) and competitive with Si−C photocleavage certainly cannot be ruled out.

The somewhat greater complexity and higher exposure dose associated with PYR SAM patterning and metallization requires the development of alternative ligand SAM systems exhibiting lower exposure doses and compatibility with Sn-free Pd catalysts. The PEDA SAM (Scheme 1), which comprises both metal chelating ethylenediamine and benzyl chromophore components, provides one such system. Unlike the pyridyl chromophore of the PYR SAM, the PEDA benzyl chromophore strongly absorbs 193-nm light ($\varepsilon_{193} \cong 4.7 \times 10^4$ cm^2 · mol^{-1}) (40). However, its UV photochemistry is complicated by the formation of photoproducts originating from both Si−C photocleavage and benzylic C−N photocleavage during 193-nm exposure (28). Benzylic C−N scission (∼67%), leading to the formation of a surface-bound benzaldehyde species that can undergo further photodegradation, dominates Si−C cleavage (∼33%), as shown in Figure 6A. In addition, no photoproducts are ejected from the surface in this case, in contrast to the behavior noted for the simple aromatic siloxane and PYR SAMs. Initial photoproducts remain adsorbed to the surface, presumably via hydrogen bonding with the remaining intact ethylenediamine sites in the SAM. There they are subject to further UV degradation, leading eventually to simpler photoproducts that can be desorbed from the surface.

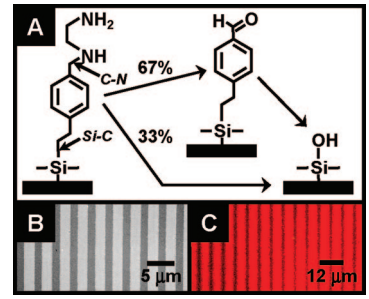

FIGURE 6. Patterning PEDA SAMs: (A) 193-nm UV photochemistry of PEDA SAM; (B) EL Ni features (light areas) prepared via the scheme of Figure 5A using PEDA SAM; (C) fluorescent Cy 3.5 dye patterns (red) formed by selective covalent binding of dye to intact alkylamine sites of PEDA SAM remaining in unirradiated regions after patterned UV exposure.

Complete degradation of the initial PEDA SAM and its adsorbed photoproducts requires a 193-nm exposure dose of ∼1.2 J · cm^{-2}, leaving a surface comprising free silanol groups (40). Fortunately, however, this dose can be significantly lowered if the initial Si−C and benzyl C−N photocleavage products are removed from the surface immediately after formation via an aqueous rinse. In this manner, equivalent spectroscopic and metallization exposure doses of just ∼350−400 mJ · cm^{-2} have been determined for the PEDA SAM on fused silica at 193 nm (28). This exposure dose is comparable to the ∼400 mJ · cm^{-2} spectroscopic dose observed for phenylsiloxane and related aromatic siloxane SAMs. However, it is clearly superior to the ∼500−800 mJ · cm^{-2} metallization doses required for aromatic siloxanes using Pd−Sn catalysts, consistent with expectations given the differences in the binding mechanisms and specificities between the Pd−Sn and Sn-free Pd catalyst systems.

One such example of a low-resolution UV-patterned PEDA SAM on a Si wafer substrate after selective Ni plating is shown in Figure 6B. Higher-resolution features in Ni having widths as small as ∼15 nm are readily prepared using PEDA SAMs patterned with proximal probe exposure tools (24, 55). In addition, because the alkylamine components of the PEDA SAM possess a wider range of reactivity than the pyridyl N site of the PYR SAM, they are capable of covalently binding materials other than Pd catalysts or EL metal. Consequently, patterned PEDA SAMs can also be used to selectively and covalently bind dyes (Figure 6C) or DNA (28, 41) that retain their function for biological or other applications.

PEDA SAMs provide the most efficient ligand organosiloxane SAM systems currently available for 193-nm patterning using our TSI approach. However, the PEDA exposure dose of ∼350−400 mJ · cm^{-2} greatly exceeds the <10 mJ · cm^{-2} dose using conventional photoresists required for sufficient throughput in a manufacturing process. In addition, because patterning using PEDA relies on the destruction or removal of the alkylamine ligand, only positive-tone metal patterns that replicate the patterning mask can be obtained. Attempts to develop ligand chromophores having improved UV absorbance (45) at 193 nm have failed to provide materials having exposure doses <400 mJ · cm^{-2}. Although

Downloaded by 194.44.31.30 on November 3, 2009 | http://pubs.acs.org
Publication Date (Web): January 12, 2009 | doi: 10.1021/am800121d

Downloaded by 194.44.31.30 on November 3, 2009 | http://pubs.acs.org
Publication Date (Web): January 12, 2009 | doi: 10.1021/am800121d

Scheme 2. Structures of Benzyl Chromophores

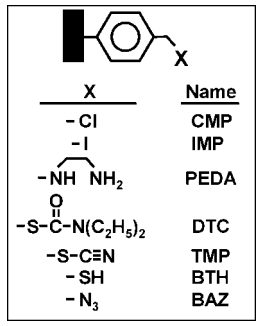

vacuum UV (i.e., VUV; $\lambda < 190$ nm) exposures can access higher excited states of SAM organofunctional groups (146−148) that can initiate new and potentially more rapid photodegradation pathways, the appropriate exposure tools are not yet widely available. Consequently, there exists a pressing need for the development of new SAMs amenable for TSI and selective EL plating that are capable of providing both positive- and negative-tone images at lower exposure doses.

III-C. (Chloromethyl)phenyl (CMP) Chromophores for TSI and EL Plating. We have pursued solutions to this problem by again using a "divide and conquer" approach. In this case, we partition the imaging and ligating functions of the ligand SAM to optimize each function separately. Specifically, an organofunctional group capable of undergoing photoreactions at low exposure doses, but not able to ligate a metal ion, is selected for use as the organosiloxane SAM. Following patterning, a ligand group is covalently and selectively grafted to either, but not both, the surface photoproduct(s) generated during exposure or the intact organofunctional groups remaining on the unexposed portions of the SAM to fabricate a negative- or positive-tone ligand pattern, respectively. Although the ligand grafting requirement adds a processing step, the tradeoff is acceptable if grafting can be performed rapidly (i.e., minutes) under aqueous, ambient conditions to preserve the gains in throughput afforded by the faster photospeed imaging step. Subsequent covalent binding of a Sn-free Pd colloid to the ligand pattern, followed by EL plating, once again fabricates the desired metal features.

III-C1. CMP Photochemistry. The CMP (Scheme 2; X = Cl; also known as benzyl chloride) chromophore has long been exploited as a component of photoresist polymers because of its well-documented sensitivity to electrons, ions, X-ray, or UV radiation (149−152). Exposure under vacuum or inert atmosphere conditions employed during commercial patterning processes leads to the formation of benzyl radicals, which effectively cross-link the film and reduce its solubility during subsequent development steps (153). The first attempt to study the UV photochemistry of the CMP group under ambient conditions was made in 1997 by Doppelt (154), who reported the formation of a surface carbonyl band at ∼1725 cm^{-1} during deep-UV exposure of [(chloromethyl)phenyl]siloxane SAMs in air. We have subsequently characterized the photochemistry at 248 nm ≥ λ ≥ 193 nm for both [(chloromethyl)phenyl]siloxane SAMs (31, 39, 155) and poly[(chloromethyl)styrene] thin films (31, 32). In this wavelength range, exposure leads to the initial loss of Cl as HCl gas. Photolysis is accompanied by the formation of a broad IR band near ∼1700 cm^{-1} characteristic of surface carbonyl species, which is >95% complete during 193-nm exposure after doses of ∼50 and ∼100 $mJ \cdot cm^{-2}$, respectively, for the [(chloromethyl)phenyl]siloxane SAM and poly[(chloromethyl)styrene] film.

Deconvolution of the carbonyl band reveals the presence of both surface benzaldehyde (1700 cm^{-1}) and benzoic acid, which appears at ∼1685 cm^{-1} (non-hydrogen-bonded dimer) for the 2D [(chloromethyl)phenyl]siloxane SAM and at ∼1725 cm^{-1} (hydrogen-bonded dimer) for the 3D poly[(chloromethyl)styrene] film, in a ∼70:30 ratio, respectively, in the limit of a zero exposure dose. The oxygen in the surface photoproducts is derived from atmospheric oxygen, as shown by (1) a general decrease in the amounts of surface photoproducts as atmospheric oxygen levels are lowered and (2) the lack of any carbonyl IR band position shift (2 cm^{-1} resolution) following isotopic substitution of $H_2{}^{18}O$ for $H_2{}^{16}O$ during the exposure (143). At 193 nm, continued irradiation leads to oxidation of the initial aldehyde formed to carboxylic acid by ozone generated during photolysis in air.

III-C2. Covalent Ligand Grafting for CMP TSI. Among the species remaining on the CMP surface after UV patterning, the CMP and benzaldehyde functional groups do not ligate the anionic Pd^{II} colloidal species required for EL plating at all, while the minor benzoic acid photoproduct binds only weakly (156). Therefore, grafting of a strong Pd^{II} binding ligand to either the benzaldehyde−benzoic acid photoproducts formed in the irradiated surface regions or the intact CMP groups remaining in the unirradiated areas is required to promote selective EL metallization. For example, reductive amination of the benzaldehyde photoproduct via reaction with ammonium acetate in the presence of a reductant such as sodium cyanoborohydride selectively transforms the aldehyde into a benzylamine ligand (32, 39) capable of efficiently binding Pd^{II} colloidal catalysts. The reaction is carried out in an aqueous or aqueous alcohol solution at pH ∼4−6 under ambient conditions, as required for a manufacturing process. Fabrication of negative-tone EL metal features using this approach is illustrated by the process sequence of path A in Figure 7A and the corresponding Ni features in Figure 7B. Analogous amine grafting chemistry can be carried out on CMP films patterned using proximity X-rays (i.e., $\lambda = 0.9385$ nm), suggesting that photochemistry similar to that observed for the UV occurs, albeit at higher exposure doses (50, 157).

The fabrication of analogous positive-tone Ni features requires selective grafting of a ligand to the intact CMP functional groups remaining in the unirradiated regions of the film, as illustrated by the process scheme in path B of Figure 7A. Although the CMP group is generally unreactive under aqueous, ambient conditions, it is an efficient alkylating agent in dry, aprotic solvents (152, 158−161). For example, alkylation of the lithium salts of an ethylenediamine anion or a 3-pyridyl anion by the CMP group readily

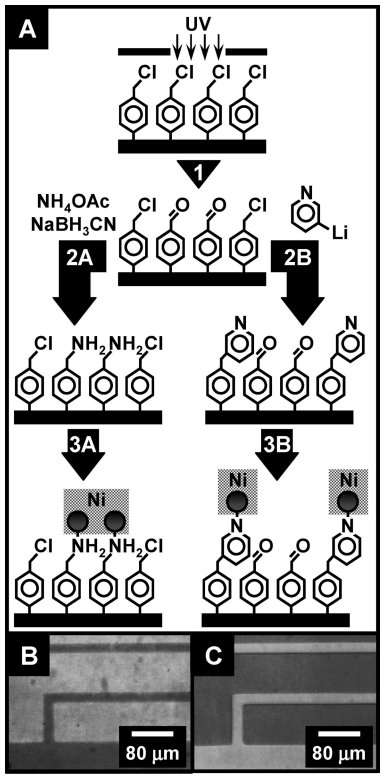

FIGURE 7. CMP chromophores for versatile TSI layers: (A) schemes showing the formation of negative-tone (path A) and positive-tone (path B) metal features via selective amine ligand grafting to aldehyde or CMP groups in irradiated or unirradiated CMP film regions, respectively; (B) negative-tone Ni feature (light areas) prepared according to path A; (C) positive-tone Ni features (light areas) prepared via path B.

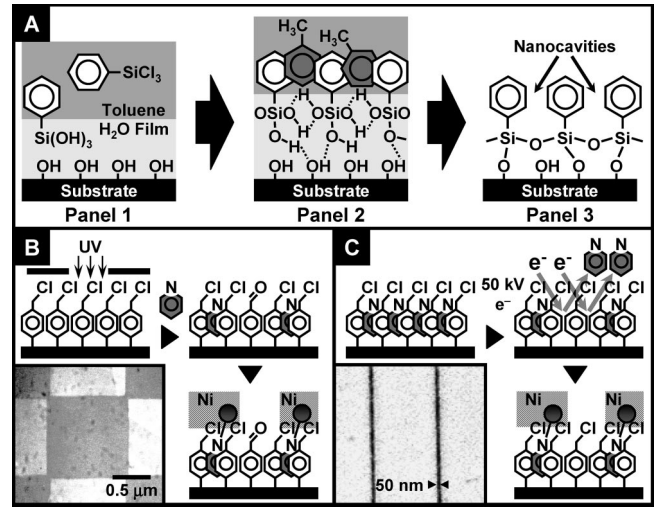

FIGURE 8. Noncovalent approach for positive-tone metallization: (A) aromatic organosiloxane chemisorption model leading to aromatic organosiloxane SAMs bearing nanocavities suitable for noncovalent ligand inclusion and EL plating; (B) UV nanocavity patterning approach for CMP-based films showing selective ligand inclusion and EL plating. Inset: EL Ni (light areas) checkerboard features prepared via the scheme in part B; (C) patterning and selective EL plating scheme based on 50 keV e-beam pyridine ligand displacement from CMP film nanocavities. Inset: ~50-nm-width lines fabricated in Ni metal (light areas) using the scheme in part C.

occurs in a dry *N*,*N*-dimethylformamide (DMF) solution at room temperature, selectively grafting these ligands to the unexposed regions of CMP-bearing films (45, 49, 152). The ligand-modified films so obtained selectively bind Pd^{II} colloids and catalyze EL plating, producing the desired complementary positive-tone Ni serpentine features shown in Figure 7C.

III-C3. Noncovalent Ligand Grafting for CMP TSI. Although positive-tone Ni features are readily formed via the grafting technique of path B in Figure 7, the reaction conditions preclude its economic use in a manufacturing environment. A viable aqueous alternative exploits the ability to control the packing density in organosiloxane SAMs or polymer chains during film formation to create sites for the noncovalent binding of ligands (23, 29–31, 33, 63, 71, 162). For example, Figure 8A illustrates the chemisorption process for aromatic siloxane SAMs. In this model (29, 31), an aromatic trichlorosilane is hydrolyzed to the corresponding trisilanol at a hydroxylated substrate surface by adsorbed water (panel 1). The nascent SAM is stabilized primarily by hydrogen bonding of its trisilanol groups with surface hydroxyl groups and adjacent trisilanol species (panel 2). However, additional noncovalent interactions among the film's aromatic groups or between its aromatic groups and solvent molecules can provide further stabilization. In general, strong $\pi-\pi$ interactions between adjacent aromatic groups in the film are expected to occur, leading to a close-packed SAM as the hydrogen-bonded network condenses to form a covalently linked siloxane on the surface. In the presence of an aromatic solvent such as toluene, however, $\pi-\pi$ interactions between the excess solvent and the film's aromatic functional groups occur competitively, leading to solvent intercalation within the film (panel 2). Subsequent expulsion of intercalated solvent occurs during siloxane bond formation, yielding a less densely packed SAM bearing solvent-templated nanocavities (panel 3) (63).

We have demonstrated that these solvent-templated nanocavities provide convenient sites for the reversible, noncovalent adsorption of ligands useful for our EL metallization processes (29, 31, 33). Because adsorption is driven primarily by the stabilization of hydrophobic portions of the ligand structure within the hydrophobic nanocavities, hydrophilic sites responsible for binding metal ions generally remain accessible to the aqueous solution after adsorption. For example, dimethylamine and pyridine readily partition into a toluene-templated CMP SAM from aqueous solution, where each binds sufficient PD1 catalyst to support EL Ni deposition (29). However, whereas pyridine is able to form strong $\pi-\pi$ interactions with the aromatic nanocavity sidewalls, dimethylamine cannot. Therefore, dimethylamine is readily displaced prior to catalyst treatment by (1) rinsing with an acidic aqueous solution, which protonates its N site and increases its hydrophilicity, or (2) treatment with toluene, which binds more strongly inside the nanocavities via $\pi-\pi$ interactions. In contrast, the $\pi-\pi$ interactions between the pyridine ligand and the nanocavity sidewalls are sufficiently strong to prevent its extraction in an acid solution or toluene. Nevertheless, exposure of films to high-vacuum conditions overnight extracts the pyridine, confirming its noncovalent association with the film.

Downloaded by 194.44.31.30 on November 3, 2009 | http://pubs.acs.org
Publication Date (Web): January 12, 2009 | doi: 10.1021/am800121d

Downloaded by 194.44.31.30 on November 3, 2009 | http://pubs.acs.org
Publication Date (Web): January 12, 2009 | doi: 10.1021/am800121d

Ligand adsorption can be spatially controlled via several patterning methods. For example, μCP using hydrogel stamps charged with an aqueous ligand solution as the ink can selectively insert N ligand species such as pyridine (61) or Starburst PAMAM amine dendrimers (59) into the nanocavities of CMP SAMs. Excess ligand solution delivered to the surface during the stamping process is removed by gentle heating, which evaporates the solvent and promotes ligand alkylation by surface CMP groups (61), chemically fixing the pattern to the surface. Subsequent selective covalent attachment of a fluorescent dye or PD1 catalyst and EL Ni has been demonstrated (31, 59, 61). However, the mechanical properties of the hydrogel stamp (59, 60) currently limit this process to the fabrication of microscale features.

Spatial control of ligand adsorption using conventional patterning tools is shown in parts B and C of Figure 8. For example, hydrophilic aldehyde and carboxylic acid surface photoproducts generated during UV exposure of the CMP SAM in Figure 8B inhibit subsequent pyridine incorporation into the underlying nanocavities. Sufficient pyridine is adsorbed only by accessible nanocavities present in the unexposed film regions, leading to selective binding of the PD1 catalyst and deposition of the positive-tone EL Ni features (29, 31, 33) shown in Figure 8B (inset). Analogous metal features can be fabricated using X-rays (29, 31, 157) or low-energy electrons (23) from the tip of a scanning tunneling microscope for film patterning. In a similar fashion, high-energy e-beams efficiently displace the strongly physisorbed pyridine ligand from CMP SAM nanocavities (23, 29, 31, 63), as shown in Figure 8C. Treatment of the resulting ligand template with the ultrasmall, near-monodisperse PD0 colloids permits selective deposition of the positive-tone Ni film shown in Figure 8C (inset). The ~50-nm-width lines created in the Ni metal exhibit sufficient control of the feature edge acuity to satisfy the 5% design rule concerning permissible feature width variations for electronics circuit fabrication (29, 63).

IV. CHANNEL-CONSTRAINED METALLIZATION (CCM)

Although our TSI process can readily fabricate the sub-100-nm features required for nanoelectronics applications, several challenges remain before it can be implemented in the manufacturing environment. For example, the best available CMP SAMs and thin polymer films currently used as imaging layers require exposure doses (i.e., ~50 mJ · cm^{-2} for 193-nm UV exposures) that still exceed those of conventional photoresists (e.g., < 10 mJ · cm^{-2} for UV exposures), limiting sample throughput. In addition, the reproducible fabrication of uniformly thick organosiloxane SAMs useful as imaging layers, especially from moisture-sensitive trichlorosilane precursors (63), presents a potential manufacturing challenge. Finally, undesirable lateral growth of metal due to the isotropic nature of the EL growth process limits the thickness of metal that can be deposited onto the patterned surface without compromising the feature fidelity, especially for the densely packed nanoscale features (14) increasingly required for advanced electronics applications.

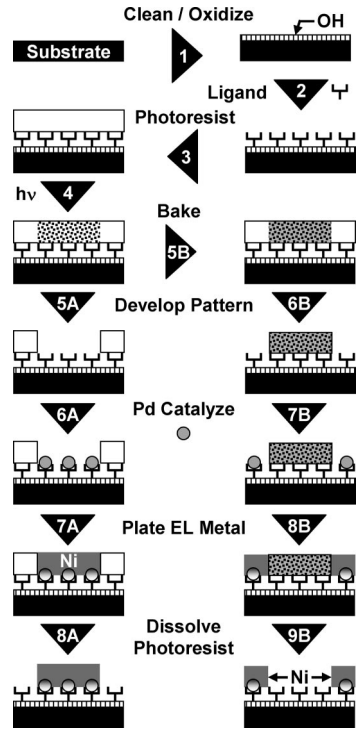

FIGURE 9. CCM approach for patterned metallization. The tone of the metal pattern is determined by the type of photoresist used. A negative-tone metal pattern is fabricated via path A if exposure of a photoresist in step 4 increases the resist solubility during development in step 5A. Positive-tone metal features are fabricated via path B if exposure ultimately leads to photoresist cross-linking. For example, certain chemically amplified resists generate acid during exposure, which can catalyze resist cross-linking during a postexposure bake shown in step 5B. The cross-linked resist remains after development in step 6B, producing a polymer structure of tone opposite to that formed via path A. Further processing leads to the deposition of a positive-tone metal pattern that complements the negative-tone metal pattern of path A.

Although lower-dose SAMs will likely become accessible through synthesis or the use of shorter patterning wavelengths (146, 148, 163−166), more reliable vapor-phase deposition (160) techniques may supplant solution-based SAM chemisorption, and lateral metal growth issues may be addressed by anisotropic EL metal deposition methods (167−169), their compatibility with current manufacturing processes has not been conclusively demonstrated. Therefore, other options for selective EL metal deposition of patterned substrates also need to be explored.

One such alternative, known as CCM (34−36, 38, 43, 170), utilizes photoresist−SAM composite films for fabrication of both positive- and negative-tone patterned metal features. An appropriate photoresist is spin-coated onto a substrate bearing a chemisorbed ligand organosiloxane SAM, as shown in Figure 9. Exposure leads to chemical changes that increase (path A) or decrease (path B) photoresist solubility during a subsequent development step, which selectively uncovers the ligand SAM to define a pattern. Covalent binding of a colloidal Pd catalyst to the ligand selectively initiates EL metallization within the pattern channels. Dissolution of the photoresist following plating leaves the desired negative-tone (path A) or positive-tone (path B) metal pattern.

Downloaded by 194.44.31.30 on November 3, 2009 | http://pubs.acs.org
Publication Date (Web): January 12, 2009 | doi: 10.1021/am800121d

The CCM process offers several manufacturing advantages. First, because the photoresist performs the imaging function, the range of useful ligand SAMs is greatly expanded. For example, a simple ligand such as EDA (Scheme 1) can be used because the ligand need not contain a chromophore as part of its structure. Alkylamine ligands such as EDA are particularly useful because they are soluble in water or simple alcohols and are amenable for chemisorption onto hydroxyl-bearing substrates via microelectronics-compatible spin-coating procedures (38). Second, lateral growth of EL metal is confined by the photoresist channel walls, permitting fabrication of high-aspect-ratio metal structures appropriate for use as plasma-etch-resistant masks, diffusion barriers, or electrical interconnects (36, 170). Third, a variety of photoresists sensitive to UV, X-ray, or e-beam exposure can be employed, with the photoresist−SAM combination selected to control the photoresist and development residue adhesion to the SAM and optimize the image quality (35). Finally, the photoresist thickness can be adjusted during spin-coating to compensate for depth-of-focus and transparency issues, if necessary, because the photoresist is not subjected to plasma etching during processing. Pinhole-free polymer films as thin as ~50−100 nm (32) can readily be prepared as imaging layers, as required. In addition, advanced photoresists exhibiting enhanced UV transparency are increasingly available (171), as required for the fabrication of higher aspect ratio metal structures useful as electrical interconnects.

Parts A−D of Figure 10 (172) illustrate the use of the CCM process for fabrication of metal features of increasingly higher resolution on substrates of decreasing surface roughness. For example, Ni metal features of ~10- and 50-μm (inset) widths, prepared on an alumina circuit board substrate, are shown in Figure 10A (34, 36). The ~6-μm-thick Ni features adhere well (inset) and conform to the rough topography of the alumina substrate. Microscale resolution Ni features (~250-nm-thick) are also readily fabricated on smoother polyimide films after O_2 plasma etching to generate surface hydroxyl sites for SAM chemisorption, as shown in Figure 10B. Figure 10C shows a Siemens's star pattern bearing a ~100-nm-thick Ni film on a Si wafer after RIE pattern transfer into the Si. The ~0.6-μm Si etch depth, together with the vertical Si sidewalls and smooth Si channel floors, is sufficient for use of the etched sample after Ni removal as a master for casting polymer stamps required for μCP (59, 60). Because Ni exhibits an etch selectivity of nearly 200:1 compared to Si, features as deep as ~19−20 μm can be fabricated during the RIE step before breakthrough of the ~100-nm-thick Ni mask occurs (19). Finally, Figure 10D shows two examples of high-resolution features fabricated via the CCM process using high-energy extreme UV (i.e., EUV; $\lambda \cong 11-14$ nm) and e-beam (inset) exposure tools. The nominal 0.20-μm feature highlighted is plated as a ~90-nm-thick Ni feature of width ~0.227 μm on a polymer planarizer using a photoresist whose thickness (~70 nm) has been adjusted to compensate for EUV transparency issues. The increased width of the Ni feature (0.227 μm) compared

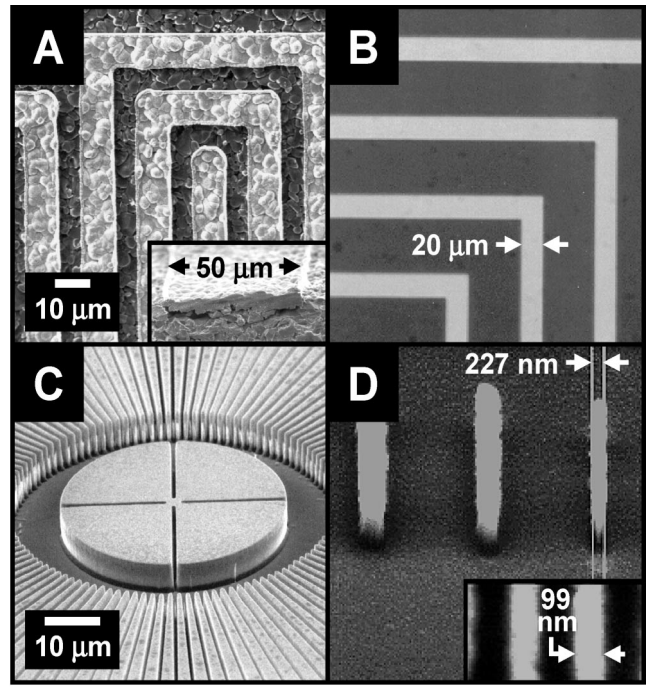

FIGURE 10. Ni features (light areas) prepared via CCM: (A) optical micrographs of Ni features on alumina with a Ni line cross section (inset); (B) optical micrograph of Ni lines on polyimide; (C) SEM of Ni features on Si after RIE pattern transfer into the Si substrate; (D) SEMs of EUV-patterned Ni features on a cross-linked planarizer layer on Si after RIE pattern transfer and 50-kV e-beam-patterned Ni gratings on Si (inset). The ~100-nm Ni gratings in Figure 10D (inset) are reproduced with permission from *Thin Solid Films* 2000, *379*, 203. Copyright 2000 Elsevier Science Publishing. Processing conditions are described in ref 172.

to the printed photoresist pattern (0.20 μm) is consistent with the resumption of lateral Ni growth after the thickness of the Ni feature exceeds the photoresist channel height (70 nm). Nevertheless, these Ni features successfully resist degradation during O_2 RIE pattern transfer through the planarizer layer to the Si substrate. Finally, the ~100-nm-width Ni gratings on Si shown in Figure 10D (inset), prepared using a high-energy e-beam patterning tool, demonstrate the ability of the various CCM process steps to function effectively to fabricate features at the nanoscale (35). The "mushrooming" effect noted for the Ni features produced via the EUV process in Figure 10D is not observed for these features because the plated Ni thickness (~15−20 nm) is less than the photoresist thickness (~0.30 μm).

V. PROCESS EXTENSIONS AND CHALLENGES

Although we have demonstrated nanoscale feature fabrication feasibility for both the TSI and CCM methods using Sn-free Pd catalysts, various challenges remain before the processes can be transitioned to a manufacturing environment. For example, the stability and shelf life must be improved, especially for Pd^{II}-based catalysts, to meet general manufacturing requirements of at least ~6 months. In addition, further decreases in the average catalyst particle size and polydispersity will clearly be required to maintain acceptable control of feature critical dimensions during metallization as feature sizes shrink below ~10 nm and ultimately approach molecular dimensions. For patterned

Downloaded by 194.44.31.30 on November 3, 2009 | http://pubs.acs.org
Publication Date (Web): January 12, 2009 | doi: 10.1021/am800121d

metallizations involving TSI imaging, SAM or polymer film exposure doses must be lowered by at least a factor of ~5 from the current values to maintain sample throughput. Although current ligand grafting processes associated with the nonligand benzyl chromophore imaging films satisfy requirements for selectivity and aqueous, ambient reaction conditions, ligand binding times of typically >1 h must be substantially reduced (i.e., ~2 min) to improve sample throughput. In a similar fashion, current CCM processes possess the low exposure doses, as well as the photoresist adhesion to and the ability to clear developed photoresist residue from the underlying ligand SAM, required for fabrication of metal features having sizes as small as ~100 nm. As features become even smaller, however, more stringent requirements in these areas will test the ability of the CCM process to fabricate metal features with acceptable fidelity. Therefore, we conclude this paper with discussions of related efforts regarding further process testing and optimization for manufacturing use, as well as process extensions and issues related to the fabrication of sub-50-nm metal features.

V-A. Catalyst Alternatives. The development of Sn-free EL Pd catalysts described here has spurred efforts elsewhere to further test their applicability for the fabrication of metal structures useful for electronics and address the stability and size issues associated with their use. For example, Osaka and co-workers (18, 173−177) have shown that EL Ni films fabricated using Sn-free colloidal catalysts in a ligand SAM approach function as efficient Cu diffusion barriers. Ni films have been deposited using PD1 (173), as well as Na-free $PdCl_2$-based catalysts (18, 177) amenable for CMOS device manufacture. The Ni films remain adherent at processing temperatures as high as ~400 °C (173−175), indicating that the underlying SAM remains intact, in contrast to the poor thermal stability of SAMs in air (178) but comparable to their thermal stability in a vacuum (179). In related work, ligand SAMs alone have been shown to function as effective adhesion promoters (180, 181) and diffusion barriers (182−185) for Cu metal, as demonstrated by the fabrication of functional MOS capacitors using ligand SAM templates. At Nagoya University, Koumoto and co-workers (105, 186−188) have pioneered the use of both Pd−Sn and PD1-type Sn-free catalysts for patterned EL deposition of oxide features, such as ZnO and In_2O_3, useful for optoelectronics applications. Meanwhile, Bittner and co-workers have utilized PD1 for selective EL Co plating of μCP-patterned PAMAM amine dendrimer ligands on bare Si wafers (189) and developed PD1 analogues capable of selectively plating the interior of a tobacco mosaic virus template, affording continuous EL Co or Ni nanowires having diameters as small as ~3 nm (190, 191). The use of other colloidal PD1 derivatives, prepared via hydrolysis of palladium(II) salts in pH ~2.5−7.0 aqueous solutions containing various amounts of added chloride ion, has also been reported for EL metallization of ZnO (192), lipid cerasome membrane (193, 194), chitosan (116−118), aminosiloxane SAM−diamond (165), and aminosiloxane-modified (147) or amine plasma-modified (195) polyimide films.

V-A1. Pd^{II} Hydrolysis Control for Colloidal Catalysts. Issues regarding improved control of colloidal catalyst stability, shelf life, size, and polydispersity have also received increased attention in recent years. Several approaches are currently being pursued. The first involves control of the Pd^{II} hydrolysis chemistry through adjustments in the solution pH and chloride ion levels or catalyst formation and storage conditions to control both the colloid size and stability. For example, we have exploited the temperature sensitivity of Pd^{II} hydrolysis reactions to increase the lifetime of our active PD2 catalyst from ~1 day to ~1 week via storage at ~4 °C (143). In addition, Boily and co-workers (127) have performed extensive studies of the Pd^{II} hydrolysis chemistry in weakly acidic aqueous solutions containing high chloride levels. Although their observations indicate that Pd^{II} nanoparticles stable for up to ~1 year can be prepared, such particles have not yet been tested to determine whether they possess the requisite ligand-binding selectivity and catalytic activity for EL plating applications. However, consistent with these observations, Xu and co-workers (196−198) have reported the use of "chloride-rich" Pd^{II}-based colloids having sizes of ~6 nm and shelf lives >6 months for EL plating using ligand SAMs similar to those described here. Unfortunately, the details presented to date concerning the preparation of these catalysts are insufficient to ascertain their composition, structure, or other properties.

Concentrated (i.e., greater than millimolar) $PdCl_2$-based formulations in alcohol (199) or strongly acidic (pH ≤0) HCl(aq) solutions provide an alternative means to control catalyst properties. The characteristic bis(μ-chloro)-bridged oligomeric structure of $PdCl_2$ (156) is at least partially preserved under these conditions, permitting binding of sufficient Pd^{II} by surface ligands for EL plating (18, 177, 200−204). Catalyst stability is generally improved because the Pd^{II} hydrolysis reactions (e.g., eqs 1−4) responsible for colloid agglomeration at higher pH in aqueous solutions are inhibited. In addition, because alkali-metal ions such as Na^+ affect the performance and lifetime of CMOS devices (13), these Na-free formulations are preferred for electronics applications.

V-A2. Monomeric Pd^{II} Species as Catalysts. Because of their molecular size, several efforts to utilize monomeric Pd^{II} transition-metal complexes as EL plating catalysts have also been initiated. The use of discrete Pd^{II} species for EL plating requires (1) the coordination of ligands directly to the Pd^{II} site and/or (2) the use of solution conditions that are capable of arresting the hydrolysis reactions leading to oligomer or colloid formation. In addition, because SAMs cannot bind sufficient monomeric Pd^{II} species to sustain the EL process, 3D ligand polymer films are typically utilized to bind the additional Pd^{II} required.

Stabilizing ligands are typically chosen from strong σ-donor species such as ammonia, alkylamines, or carboxylates, which bind Pd^{II} and stabilize the resulting monomeric complex in solution. However, the complex formed may no longer possess labile coordination sites necessary to covalently bind a surface ligand for EL plating. Therefore, charged monomeric Pd^{II} complexes are usually employed

Downloaded by 194.44.31.30 on November 3, 2009 | http://pubs.acs.org
Publication Date (Web): January 12, 2009 | doi: 10.1021/am800121d

to permit binding to surface ligands via electrostatic and hydrogen-bonding interactions. Because the nascent Pd^0 nanoparticles formed via the reduction of bound Pd^{II} during plating do not readily coordinate these σ-donor species, the nanoparticle surface is accessible for EL deposition. Adhesion of the metal deposit is controlled via mechanical interlocking of the growing metal deposit within the polymer chains and/or the use of polymers bearing stronger π-acceptor surface ligands capable of binding Pd^0. Examples of this approach include the use of $Pd(NH_3)_4^{2+}$ complexes as catalysts for the EL plating of charged phospholipid membranes (205) and polyacrylate multilayer films (206, 207).

Analogous results can be obtained using simpler labile palladium(II) salts in solutions that inhibit hydrolysis. For example, the treatment of chitosan thin films (117, 118) with $PdCl_4^{2-}$ in pH ~1 HCl(aq) binds sufficient Pd^{II} for EL plating. Kang and co-workers (208−214), among others (215), have extended the use of simple palladium(II) salt solutions in pH ~1 HCl(aq) or HNO_3(aq) to catalyze EL plating of ligand polymer brushes. Brushes are readily grown from substrate surfaces modified via plasma (209, 210, 213), photochemical (211, 214), or chemical (208, 212, 215) reactions through oxidative graft copolymerization, UV-induced polymerization, and atom-transfer radical polymerization of ligand monomers or their precursors. Substrates relevant for electronics applications, including polyimide (212, 213), SiLK dielectric (210, 213), poly(tetrafluoroethylene) (PTFE) (209), glass (208), and Si wafers (211, 214, 215), have been plated with excellent adhesion of the EL metal deposits.

V-A3. Pd-Free Catalysts. The successful demonstration of monomeric Pd^{II} complexes as EL catalysts with ligand polymer substrates has also increased interest in the development of Pd-free catalysts as a means to reduce both the cost and environmental footprint of the plating process. Au (58, 216) or Ag (217) nanoparticles are well-known EL catalysts and can substitute for Pd in this role. However, recent demonstrations of the EL activity of fresh Cu nanoparticles (218, 219) have spurred interest in the development of catalysts derived from less-noble metals. For example, Bicek and Karagoz (220) have described a method for the metallization of polystyrene in which initial chlorosulfonation and reaction with hydrazine form a sulfonyl hydrazide surface ligand that binds Cu^{II} directly. Subsequent reduction generates Cu^0 seeds that catalyze EL Cu deposition. Whang and co-workers (221) have hydrolyzed polyimide to create surface carboxylate ligands that bind Ni^{II}, which can be reduced to form Ni^0 seeds that catalyze EL Ni deposition. In analogous work, Charbonnier, Romand, and co-workers (222, 223) have plasma-grafted amine ligands to various polymers to directly bind Ni^{II} or Cu^{II} species. Subsequent H_2 plasma (222) and VUV (223) reduction to Ni^0 and Cu^0, respectively, produces metal seeds that catalyze EL plating.

Ligand SAMs have also been used, in conjunction with simple Cu^{II} complexes, for EL plating. For example, Zangmeister and van Zee (224) have reported spontaneous EL Cu deposition during treatment of a *p*-thiobenzoic acid SAM on a Au substrate with an EL bath comprising a copper(II) tartrate complex and formaldehyde. Lu and Walker (225) have similarly observed EL Cu deposition on ω-mercaptohexadecanoic acid SAMs on Au substrates using a Cu^{II}EDTA EL bath containing formaldehyde. Weak Cu^{II}−surface carboxylate interactions have been confirmed in both cases. We note that this behavior contrasts with that described in section II-B for monomeric Pd^{II} species bound to mercaptopyridine SAMs on Au substrates (124). In that case, loss of metallic behavior in the reduced Pd^0 state due to a reduction in the density of states near the Fermi level promoted by the coordinated ligand quenches EL plating. Consequently, the behavior of copper(II) carboxylate systems suggests that other surface-ligated metal ions retaining sufficient metallic behavior to catalyze EL plating after reduction to the zerovalent metal state may exist.

Pd-free EL plating can also be accomplished by using the substrate as the reductant to directly reduce metal ions to metal particle seeds capable of catalyzing further metal deposition in an EL bath. For example, in a basic solution at elevated temperatures, hydrogen-terminated Si is readily oxidized to SiO_2, releasing H_2 and electrons that readily reduce Cu^{II} or Ni^{II} ions to the corresponding metals (226−228). Osaka and co-workers (229−231) have demonstrated that suboxides of silicon (i.e., SiO_x, $x < 2$) formed during the oxidation process can also be used to reduce metals. Using a simple TSI process, they have created silicon suboxides in an alkyl SAM chemisorbed to hydrogen-terminated Si via e-beam patterning in the presence of trace O_2 or H_2O. The silicon suboxides efficiently bind Ni^{II} ions, producing Ni^0 seeds that catalyze selective EL metallization of ~80-nm-diameter Ni dot features (230).

V-B. TSI Photochemistry. The development of new EL catalysts capable of plating nanoscale features with high fidelity and acceptable edge acuity must also be accompanied by new faster-photospeed SAMs or polymer thin film TSI layers capable of defining those features and selectively binding catalysts. Although the photochemistry of numerous SAMs in the ~248−405-nm UV wavelength range (64, 66, 120) is well-characterized, with the exception of benzyl chromophores less information is available at the 193- and ~11−14-nm wavelengths used by current UV and next-generation EUV exposure tools, respectively. Therefore, given the proven efficacy of the CMP chromophore (section III-C) for UV TSI, we restrict our discussion to materials containing other benzyl chromophores (Scheme 2) prepared via nucleophilic substitution reactions (49, 152, 232, 233) as potential low-dose imaging layers for these wavelengths.

In addition to their use at 193 nm, we have also tested several SAMs bearing benzyl chromophores as TSI layers for EUV exposure (14 nm), in conjunction with selective EL plating via ligand alkylation of unexposed benzyl chromophores (section III-C2) (45, 49). The metallization exposure dose of the CMP siloxane SAM chemisorbed onto a thermal silicon oxide wafer is ~50 mJ · cm^{-2} at 14 nm, which is equivalent to its 193-nm dose. On native silicon oxide, it increases to ~250 mJ · cm^{-2}, reflecting substrate-

Downloaded by 194.44.31.30 on November 3, 2009 | http://pubs.acs.org
Publication Date (Web): January 12, 2009 | doi: 10.1021/am800121d

dependent dose behavior similar to that discussed for UV-irradiated SAMs earlier (section III-A). A corresponding [(iodomethyl)phenyl]siloxane SAM (i.e., IMP; Scheme 2) on thermal silicon oxide exhibits a metallization dose of ~150−300 mJ · cm^{-2}, which is again comparable to the ~200 mJ · cm^{-2} value observed at 193 nm. Quantum yields for halogen atom loss at 14 nm exceed unity for both SAMs. In contrast, PEDA SAMs (Scheme 1) fail to exhibit significant chemical changes at doses <6 J · cm^{-2} during 14-nm exposure but are selectively metallized after 193-nm doses of ~350−400 mJ · cm^{-2}. These differences in behavior are consistent with established electron-induced halogen loss noted for halobenzyl chromophores (23, 234), suggesting that EUV-induced photoelectron generation at the SAM contributes to CMP and IMP SAM degradation during these exposures.

Scheme 2 shows structures of some other benzyl chromophores potentially useful as TSI layers for exposures at 193 or 14 nm. However, because their photochemistry at these wavelengths has not yet been studied, their inclusion in Scheme 2 is based on the potential for adaptation of known photochemistry at longer UV wavelengths (i.e., $\lambda \geq$ 248 nm) and/or unique covalent grafting reactions for TSI processes. For example, Matsuda and co-workers (235) have evaluated polymers containing benzyl-*N*,*N*-diethyldithiocarbamate (DTC) species as photoinitiators for surface graft polymerization of several acrylate derivatives capable of binding monomeric Pd^{II} species for EL plating. UV exposure of polymer films under a N_2 atmosphere at ~254 nm ruptures the C−S bond, forming benzyl and dithiocarbamate radicals at doses as low as ~300 mJ · cm^{-2}. In the presence of acrylate monomers, polymerization to form polyacrylates is initiated on the surface by the benzyl radical and eventually quenched by reaction of the growing acrylate polymer with the dithiocarbamate radical. Microscale patterns of various polyacrylates on the same DTC polymer film surface have been prepared via serial masked UV exposures.

Trimmel and co-workers (236−238) have also demonstrated micropatterning using polymer films bearing (thiocyanatomethyl)phenyl (TMP) chromophores. UV exposure of the TMP chromophore under a N_2 atmosphere at ~254 nm leads to C−S bond cleavage and the formation of benzyl and thiocyanato radicals. In contrast to the DTC film behavior, however, photoisomerization leading to the isothiocyanato species occurs in ~30% yield via radical recombination. The reaction of propylamine with the isothiocyanate photoproduct after exposure yields *N*-benzyl-*N*′-propylthiourea and prevents thermal isomerization to the initial thiocyanato isomer. Surface patterns of *N*-benzyl-*N*′-propylthiourea are readily prepared after UV exposure doses of only ~80 mJ · cm^{-2}. Grafting of amine PAMAM dendrimers, rather than propylamine, could in this case provide ligand sites for Pd^{II} binding and amplify the effective amine surface concentration (50, 59, 112, 189), permitting patterning at even lower exposure doses.

SAMs bearing benzylthiol (BTH) or benzyl azide (BAZ) chromophores are appealing candidates for use in our ligand metallization approach because of the chemical reactivity of their thiol and azide groups, respectively. For example, (*ω*-mercaptopropyl)siloxane SAMs having alkylthiol ligands analogous to BHT readily bind Pd^{II} colloids (197, 198) or Cu^{II} species (219) for EL plating. Unlike thiols, azides do not function as ligands for Pd species. However, their efficient Huisgen 1,3-dipolar cycloaddition reactions (239) with terminal alkynes to yield stable triazoles afford an attractive means to graft appropriate ligands to a BAZ SAM under mild conditions.

Although there are no reports describing the deep-UV photochemistry of BTH or BAZ SAMs, the behavior of analogous materials infers a rich photochemistry compatible with our ligand metallization processes. For example, photooxidation of the alkylthiol group of the (*ω*-mercaptopropyl)siloxane SAM to the corresponding sulfonate (240, 241) at 254 nm ≤ λ ≤ 193 nm occurs at doses as small as ~720 mJ · cm^{-2}, despite its poor UV absorbance. The existence of a similar BHT photooxidation process, or C−S bond photocleavage leading to H_2S ejection and a benzaldehyde surface photoproduct analogous to the CMP chromophore, would provide an effective means for patterning a BHT SAM. The potential for UV photolysis of a BAZ SAM via C−N or N−N bond cleavage is equally intriguing. C−N bond photocleavage, leading to ejection of HN_3, could generate a surface benzaldehyde photoproduct analogous to the CMP chromophore. In contrast, a N−N bond cleavage mechanism similar to that observed for phenyl azides (242) would eject N_2, leaving a highly reactive nitrene surface product. Because each of these potential photoproducts exhibits sufficient orthogonal reactivity to the parent, BTH and BAZ chromophores represent exciting new materials for the development of TSI-based selective EL plating schemes.

V-C. CCM Analogues. Although little related work has been reported directly utilizing photoresist−ligand film composites as described for the CCM process (243−245), several other groups have successfully developed variations in which the ligand film is omitted (246−249). These processes rely on direct physical or chemical interactions of species deposited in the developed photoresist channels with the uncovered substrate to create the desired material patterns. Sub-100-nm size metal features are readily fabricated in this manner via galvanic displacement reactions at a substrate surface through two such approaches. In the first, a static plowing lithography method developed by Buriak and co-workers (250) uses an AFM tip to displace photoresist film covering a redox-active substrate such as Ge(111). Spontaneous galvanic reduction of Au^{III} or Cu^{II} ions to the corresponding metals occurs at the uncovered Ge sites, creating photoresist-constrained continuous metal lines as small as ~52-nm width whose resolution is ultimately limited by the size of the AFM tip. Bhuvana and Kulkarni (251) have exploited similar substrate reactivity following high-energy e-beam patterning and the development of polystyrene thin films on native silicon oxide wafers. Treatment of the developed patterns with Au^{III} in a HF(aq) solution leads to dissolution of the uncovered SiO_2 and formation of

hydrogen-terminated Si, which efficiently reduces Au^{III} to Au metal via galvanic displacement. Features of ~80-nm width in Au metal have been fabricated.

Although sub-100-nm size features are readily prepared via AFM and e-beam techniques, sample throughput is currently limited by the serial nature of the patterning process despite ongoing efforts to develop parallel writing systems incorporating these techniques (252−254). Fortunately, soft lithography techniques such as nanoimprint lithography (NIL) (255, 256) and step and flash imprint lithography (S-FIL) (257, 258) are promising candidates for the fabrication of sub-100-nm metal features in a parallel fashion. Both techniques utilize a stamp bearing patterned features in relief, which is used to imprint a thin film coating on a substrate. The features formed in the imprinted film are analogous to those observed for CCM following patterning and the development of the photoresist. For NIL, the stamp is pressed into a polymer film heated above its glass transition temperature. The polymer flows into and fills the interstitial regions of the stamp relief features, providing a replica in the polymer film after removal of the stamp from the cooled polymer film. S-FIL utilizes a UV transparent stamp to imprint a thin film of a polymerizable liquid, which is UV-polymerized while in contact with the stamp to form a hardened polymer replica that remains on the surface after stamp removal. For both processes, a brief plasma etch is typically used to remove any polymer residue present in the channels of the patterned polymer film before further processing.

Metallization of the resulting polymer film relief structures is readily accomplished via subtractive lift-off methods. For example, metal deposited via vapor deposition techniques adheres to both the uncovered substrate and the remaining polymer template, with subsequent dissolution of the polymer conferring metallization selectivity via removal of the unwanted polymer-bound metal. Au features of ~20-nm width have been fabricated using NIL by Austin and Chou (256), and the selective deposition of Ti features of ~100-nm width has been reported by Willson and co-workers (257) using the S-FIL process. In related work, Chou and co-workers have described a photocurable NIL (P-NIL) process (259) in which sub-10-nm features are fabricated via UV-assisted imprinting of a UV-polymerizable Si-based liquid film spin-coated on a planar polymer film base layer. Subsequent RIE pattern transfer and vapor-phase metal deposition results in the fabrication of sub-10-nm-width features in Au metal.

There are no reports as yet regarding the use of solution-based EL deposition methods for the selective metallization of polymer templates prepared via standard NIL or S-FIL processes. However, Krivokapic (260) has described a NIL-type process in which a stamp bearing wedge-shaped cross-sectional relief features is used to directly imprint trenches having "V-shaped" cross sections into polymer dielectric films. Application of an EL Pd catalyst to the tips of the stamp relief structures directly and simultaneously transfers catalyst into the trench during the imprinting process. Subsequent EL Cu plating forms Cu interconnect features having widths as small as ~20−50 nm, as defined by the stamp wedge feature dimensions, directly in the trenches created in the dielectric film.

In general, however, the use of a plasma etch to remove residual polymer after imprinting via standard NIL or S-FIL techniques represents a serious impediment for ligand-based patterned EL metallization of substrates. A plasma etch will remove both the polymer residue and ligand SAM from the substrate floor in the polymer channels after imprinting, preventing binding of the Sn-free Pd catalyst required for EL plating. Attempts to deposit ligand SAM after plasma etching can also fail because the ligand may undesirably physisorb or chemisorb to the chemically altered tops and sidewalls of the remaining polymer defining the features, destroying metallization selectivity. One apparent solution to this problem is the use of a hardened cross-linked polymer planarizer layer bearing appropriate Pd^{II} binding ligands as a base coating on the substrate. Such layers are routinely required for the manufacture of CMOS devices (13) and are therefore acceptable to electronics manufacturers. For example, a planarizer layer ~100-nm thick bearing some fraction of pyridine ligands as part of its composition may retain a sufficient thickness and level of available pyridine ligand, even after a brief plasma etch to remove residual imprint polymer, to bind Pd^{II} colloids for EL plating.

A second alternative involves the solution-based removal of the residual polymer from the imprinted polymer template channels, akin to the development step of our CCM process. Huskens and co-workers (261) have recently demonstrated that such solution-based removal of the residual polymer after imprinting using the NIL technique is possible. Their removal of the residual poly(methyl methacrylate) (PMMA) via a brief acetone rinse preserves the imprinted pattern in the remaining PMMA film while uncovering reactive silanol groups of the underlying Si wafer substrate. Because the chemistry of the remaining PMMA template is not altered, selective vapor-phase chemisorption of a ligand EDA SAM to the silanols is achieved. Subsequent treatment of the patterned PMMA template with an aqueous dispersion of ~50-nm-diameter silica nanoparticles whose surfaces have been modified by anionic carboxylate species electrostatically binds the particles to protonated amine sites of EDA on the channel floor of the template. Although minimum features of only ~700-nm width have been fabricated because of the large size of the silica nanoparticles used, the work clearly (1) demonstrates the applicability of NIL for aqueous processing conditions required for EL metallization and (2) suggests that a hybrid imprint polymer−ligand SAM composite coating for the substrate analogous to those employed for CCM could be used. Similar process modifications can certainly be envisioned for S-FIL, suggesting that imprinting techniques may represent some of the most viable approaches for future fabrication of nanoscale metal features via EL processes.

Downloaded by 194.44.31.30 on November 3, 2009 | http://pubs.acs.org
Publication Date (Web): January 12, 2009 | doi: 10.1021/am800121d

Downloaded by 194.44.31.30 on November 3, 2009 | http://pubs.acs.org
Publication Date (Web): January 12, 2009 | doi: 10.1021/am800121d

VI. CONCLUDING REMARKS

In this paper, we have summarized our own and others' related efforts to develop fully additive approaches for selective EL metallization of patterned surfaces for fabrication of nanoscale metal features useful as electrical interconnects, plasma-etch-resistant masks, and diffusion barriers in electronics applications. Although the complexity of CMOS device manufacture imposes severe constraints on the choice of acceptable materials and processes (14), results reported here suggest that EL metallization techniques can be successfully adapted to satisfy these conditions. Through control of the size and polydispersity of Pd nanoparticle EL catalysts, in combination with TSI techniques, features in EL Ni as small as ~50 nm can be fabricated with sufficient control of the fidelity and edge acuity to satisfy the current 5% design rule limiting feature size variations for electronics applications (29, 63). These feature sizes are comparable to the minimum nominal ~45-nm dimensions of CMOS devices in production today (14).

Therefore, it is natural to conclude this paper by asking the question, "What are the smallest electrically conductive features that might be prepared via EL processes?" The answer, of course, is not yet known. However, recent work involving EL plating of DNA templates clearly demonstrates the ability to fabricate electrically conductive Au (262) or Ag (263) nanowires of ~15-nm diameter exhibiting ohmic behavior, with metal nanowire resistivity generally greater than that observed for bulk metal. Ohmic behavior and increased metal resistivity have also been observed by Buriak and co-workers (264) for smaller ~7-nm-wide (×9-nm-thick) Pt nanowires fabricated via plasma reduction of $PtCl_4^{2-}$-impregnated block copolymer templates. Natelson and co-workers (265) have reported similar increased metal resistivity values, as well as quantum effects at low temperatures, for even smaller ~3−5-nm-wide vapor-deposited AuPd nanowires fabricated via etching of a cleaved molecular-beam epitaxy-grown substrate template. Although comparably sized continuous Ni and Co nanowires of ~3-nm diameter have been fabricated via EL plating of the interior of a tobacco mosaic virus template (190, 191), the electrical properties of these wires have not yet been explored. Nevertheless, their successful fabrication indicates that the EL process is amenable for use in the confined nanoscale environments that will become more prevalent as feature sizes continue to shrink.

The fabrication of even higher resolution metal features will certainly require catalysts smaller than our best nearly monodisperse ~2.6-nm-diameter PD0 catalyst described here. As metal nanoparticle sizes shrink below ~1.5-nm diameter, however, metallic behavior necessary for catalysis of the EL deposition process is eventually lost because an insufficient number of metal atoms to support the formation of a metallic conduction band are present in each nanoparticle. This phenomenon may ultimately limit the minimum EL metal feature size obtainable to ~2−3 nm unless electronic interactions between neighboring sub-1.5-nm-diameter nanoparticles in a patterned surface *ensemble* (266) can be made sufficiently strong to reestablish metallic behavior. Precedent for such behavior has been observed by Nilius and co-workers (267, 268), who have noted STM electrical conductivity suggesting the formation of 1D metallic conduction bands in linear chains of Au or Pd atoms on surfaces. Although dip-pen lithography techniques are potentially capable of fabricating analogous features using metal nanoparticle (269, 270) or metal ion (271−273) inks, similar conductivity measurements using sub-1.5-nm-diameter Pd nanoparticles have not yet been reported. Consequently, the question concerning the ultimate limits of EL plating in the fabrication of nanoscale metal features for electrical interconnect applications remains unanswered. Obtaining an answer to this question and surmounting the materials and process challenges posed here for the fabrication of such nanoscale and molecular-scale metal interconnects will clearly require a concerted, sustained effort from teams of persons skilled in all major scientific and engineering disciplines.

Acknowledgment. We thank the Office of Naval Research, DARPA, and Rohm & Haas (Shipley Division) for financial support for this work under the NRL Core Funding Program, Molecular Level Large Area Printing Program, and Shipley-NRL CRADA Program, respectively. We thank Dr. G. Kubiak of Sandia National Laboratory for the EUV exposure for Figure 10D.

APPENDIX: ALPHABETICAL LIST OF ACRONYMS AND TRADE NAMES

AFM = atomic force microscopy

AZ140 = trade name for a photoresist developer from Hoechst Inc.

AZ 4620 = trade name for a photoresist from Hoechst Inc.

BAZ = benzyl azide [(azidomethyl)phenyl]

BPY = 4-[2-(trimethoxysilyl)ethyl]-4′-methyl-2,2′-bipyridine

BTH = benzylthiol [(mercaptomethyl)phenyl]

CCM = channel-constrained metallization

CMOS = complementary metal oxide semiconductor

CMP = benzyl chloride = [(chloromethyl)phenyl]

CRADA = cooperative research and development agreement

D = depth of focus

DARPA = Defense Advanced Research Projects Agency

DMF = *N*,*N*-dimethylformamide

DNA = deoxyribonucleic acid

DTC = *N*,*N*-diethyldithiocarbamatomethylphenyl = benzyl *N*,*N*-diethyldithiocarbamate

EDA = *N*-(2-aminoethyl)-(3-aminopropyl)trimethoxysilane

EDTA = ethylenediaminetetraacetic acid

EL = electroless

EUV = extreme ultraviolet, defined here as light in the ~11−14-nm wavelength range

EXAFS = extended X-ray absorption fine structure spectroscopy

Fidelity 1025 = trade name for the electroless Cu bath from OM Group, Inc.

HOAc = acetic acid

IMP = benzyl iodide = [(iodomethyl)phenyl]

IR = infrared

k, *k*′ = geometric factors for exposure tools

MF-312 = trade name for a photoresist developer from Rohm & Haas Inc.

MOS = metal oxide semiconductor

MPT = mixed potential theory

μCP = microcontact printing

NA = numerical aperture

NIL = nanoimprint lithography

NIPOSIT 468B = trade name for an electroless NiB plating bath from Rohm & Haas Inc.

NRL = Naval Research Laboratory

OAc = acetate

PAMAM = trade name for a series of poly[(amidoethyl)-ethanolamine] dendrimers from Dendritic NanoTechnologies Inc.

PD0 = near-monodisperse Pd^0-based nanoparticle electroless catalyst of ~2.6-nm average particle size prepared by the rapid reduction of Pd^{II} species in an aqueous solution

PD1 = polydisperse Pd^{II}-based nanoparticle electroless catalyst of ~30-nm average particle size prepared by the slow simultaneous nucleation and growth of hydrolyzed $PdCl_4^{2-}$ species in a slightly acidic aqueous solution

PD2 = near-monodisperse Pd^{II}-based nanoparticle electroless catalyst of ~9-nm average particle size prepared by the rapid nucleation of hydrolyzed $PdCl_4^{2-}$ species in a basic aqueous solution

PEDA = [[[(aminoethyl)amino]methyl]phenethyl]trimethoxysilane

PHOS = [(diphenylphosphino)ethyl]triethoxysilane

PMMA = poly(methyl methacrylate)

P-NIL = photocurable nanoimprint lithography

PTFE = poly(tetrafluoroethylene)

PYR = [2-(trimethoxysilyl)ethyl]pyridine

R = feature resolution

RF = radio frequency

RIE = reactive ion etch

S1400-26 = trade name for a photoresist from Rohm & Haas Inc.

SAL601-ER7 = trade name for a photoresist from Rohm & Haas Inc.

SAM = self-assembled monolayer

SEM = scanning electron microscopy

S-FIL = step and flash imprint lithography

SiLK = trade name of a low dielectric aromatic hydrocarbon polymer from Dow Chemical Co.

STM = scanning tunneling microscopy

TEM = transmission electron microscopy

TMP = benzyl thiocyanate [(thiocyanatomethyl)phenyl]

TSI = top-surface imaging

UV = ultraviolet light, defined here as light in the ~193−300-nm wavelength range

VUV = vacuum ultraviolet, defined here as light in the ~150−190-nm wavelength range

REFERENCES AND NOTES

(1) Diegoli, S.; Hamlett, C. A. E.; Leigh, S. J.; Mendes, P. M.; Preece, J. A. *Proc. Inst. Mech. Eng., Part G: J. Aerospace Eng.* **2007**, *121*, 589–629.

(2) Koh, S. J. *Nanoscale Res. Lett.* **2007**, *2*, 519–545.

(3) Ariga, K.; Hill, J. P.; Lee, M. V.; Vinu, A.; Charvet, R.; Acharya, S. *Sci. Technol. Adv. Mater.* **2008**, *9*, 014109.

(4) Kinge, S.; Crego-Calama, M.; Reinhoudt, D. N. *ChemPhysChem* **2008**, *9*, 20–42.

(5) Whang, D.; Jin, S.; Lieber, C. M. *Jpn. J. Appl. Phys., Part 1* 2004, *43* (7B), 4465–4470.

(6) Lu, W.; Lieber, C. M. *Nat. Mater.* **2007**, *6*, 841–850.

(7) Pischel, U. *Angew. Chem., Int. Ed.* **2007**, *46*, 4026–4040.

(8) Metzger, R. M. *J. Mater. Chem.* **2008**, *18*, 4364–4396.

(9) Haick, H.; Cahen, D. *Prog. Surf. Sci.* **2008**, *83*, 217–261.

(10) Park, J. H.; Ahn, B. T. *J. Electrochem. Soc.* **2003**, *150*, G6–G9.

(11) Platzman, I.; Brener, R.; Haick, H.; Tannenbaum, R. *J. Phys. Chem. C* **2008**, *112*, 1101–1108.

(12) Rodriguez, O.; Saxena, R.; Cho, W.; Plawsky, J. L.; Gill, W. N. *Ind. Eng. Chem. Res.* **2005**, *44*, 1220–1225.

(13) Madou, M. J. *Fundamentals of Microfabrication: The Science of Miniaturization*, 2nd ed.; CRC Press: New York, 2002.

(14) Willson, C. G.; Roman, B. J. *ACS Nano* **2008**, *2*, 1323–1328.

(15) Gonsalves, K. E.; Merhari, L.; Wu, H. P.; Hu, Y. Q. *Adv. Mater.* **2001**, *13*, 703–714.

(16) del Campo, A.; Arzt, E. *Chem. Rev.* **2008**, *108*, 911–945.

(17) Doppelt, P. *Coord. Chem. Rev.* **1998**, *178*, 1785–1809.

(18) Yoshino, M.; Nonaka, Y.; Sasano, J.; Matsuda, I.; Shacham-Diamand, Y.; Osaka, T. *Electrochim. Acta* **2005**, *51*, 916–920.

(19) Ma, D. I.; Shirey, L.; McCarthy, D.; Thompson, A.; Qadri, S. B.; Dressick, W. J.; Chen, M.-S.; Calvert, J. M.; Kapur, R.; Brandow, S. L. *Chem. Mater.* **2002**, *14*, 4586–4594.

(20) Zabetakis, D.; Loschialpo, P.; Smith, D.; Dinderman, M.; Dressick, W. J. *Langmuir* **2009**, in press (DOI: 10.1021/la803356y).

(21) Price, R. R.; Dressick, W. J.; Singh, A. *J. Am. Chem. Soc.* **2003**, *125*, 11259–11263.

(22) Dobisz, E. A.; Bass, R.; Brandow, S. L.; Chen, M.-S.; Dressick, W. J. *Appl. Phys. Lett.* **2003**, *82*, 478–480.

(23) Dressick, W. J.; Chen, M.-S.; Brandow, S. L.; Rhee, K. W.; Shirey, L. M.; Perkins, F. K. *Appl. Phys. Lett.* **2001**, *78*, 676–678.

(24) Brandow, S. L.; Chen, M.-S.; Wang, T.; Dulcey, C. S.; Calvert, J. M.; Bohland, J. F.; Calabrese, G. S.; Dressick, W. J. *J. Electrochem. Soc.* **1997**, *144*, 3425–3434.

(25) Dressick, W. J.; Kondracki, L. M.; Chen, M.-S.; Brandow, S. L.; Matijević, E.; Calvert, J. M. *Colloids Surf. A* **1996**, *108*, 101–111.

(26) Brandow, S. L.; Dressick, W. J.; Marrian, C. R. K.; Chow, G.-M.; Calvert, J. M. *J. Electrochem. Soc.* **1995**, *142*, 2233–2243.

(27) Dressick, W. J.; Dulcey, C. S.; Georger, J. H.; Calabrese, G. S.; Calvert, J. M. *J. Electrochem. Soc.* **1994**, *141*, 210–220.

(28) Chen, M.-S.; Dulcey, C. S.; Chrisey, L. A.; Dressick, W. J. *Adv. Funct. Mater.* **2006**, *16*, 774–783.

(29) Chen, M.-S.; Brandow, S. L.; Schull, T. L.; Chrisey, D. B.; Dressick, W. J. *Adv. Funct. Mater.* **2005**, *15*, 1364–1375.

(30) Chen, M.-S.; Dressick, W. J.; Schull, T. L.; Brandow, S. L. *Proc. SPIE* **2002**, *4608*, 155–159.

(31) Dressick, W. J.; Nealey, P. F.; Brandow, S. L. *Proc. SPIE* **2001**, *4343*, 294–305.

(32) Brandow, S. L.; Chen, M.-S.; Fertig, S. J.; Chrisey, L. A.; Dulcey, C. S.; Dressick, W. J. *Chem.—Eur. J.* **2001**, *7*, 4495–4499.

(33) Dressick, W. J.; Chen, M. S.; Brandow, S. L. *J. Am. Chem. Soc.* **2000**, *122*, 982–983.

(34) Dressick, W. J.; Dulcey, C. S.; Brandow, S. L.; Chen, M.-S.; Leonard, D. N.; Calvert, J. M.; Sims, C. W. In *Electrochemical Technology Applications in Electronics III (Proceedings of the 1999 Joint International Meeting of the Electrochemical Society)*; Romankiw, L. T., Osaka, T., Yamazaki, Y., Madore, C., Eds.; The Electrochemical Society Inc.: Pennington, NJ, 2000; Vols. *99—34*, pp 179—187.

(35) Chen, M.-S.; Brandow, S. L.; Dressick, W. J. *Thin Solid Films* **2000**, *379*, 203–212.

(36) Chen, M.-S.; Dulcey, C. S.; Brandow, S. L.; Leonard, D. N.; Dressick, W. J.; Calvert, J. M.; Sims, C. W. *J. Electrochem. Soc.* **2000**, *147*, 2607–2610.

(37) Koumoto, K.; Seo, S.; Sugiyama, T.; Seo, W. S.; Dressick, W. J. *Chem. Mater.* **1999**, *11*, 2305–2309.

(38) Chen, M.-S.; Brandow, S. L.; Dulcey, C. S.; Dressick, W. J.; Taylor, G. N.; Bohland, J. F.; Georger, J. H.; Pavelchek, E. K.; Calvert, J. M. *J. Electrochem. Soc.* **1999**, *146*, 1421–1430.

(39) Brandow, S. L.; Chen, M.-S.; Aggarwal, R.; Dulcey, C. S.; Calvert, J. M.; Dressick, W. J. *Langmuir* **1999**, *15*, 5429–5432.

(40) Dressick, W. J.; Dulcey, C. S.; Chen, M.-S.; Calvert, J. M. *Thin Solid Films* **1996**, *285*, 568–572.

(41) Chrisey, L. A.; Roberts, P. M.; Benezra, V. I.; Dressick, W. J.; Dulcey, C. S.; Calvert, J. M. In *Biomolecular Materials by Design*; Alper, M., Bayley, H., Kaplan, D., Navia, M., Eds.; Materials Research Society: Warrendale, PA, 1994; Vol. 330, pp 179—184.

(42) Calvert, J. M.; Dressick, W. J.; Dulcey, C. S.; Chen, M.-S.; Georger, J. H.; Stenger, D. A.; Koloski, T. S.; Calabrese, G. S. In *Polymers*

Downloaded by 194.44.31.30 on November 3, 2009 | http://pubs.acs.org
Publication Date (Web): January 12, 2009 | doi: 10.1021/am800121d

Downloaded by 194.44.31.30 on November 3, 2009 | http://pubs.acs.org
Publication Date (Web): January 12, 2009 | doi: 10.1021/am800121d

for Microelectronics; American Chemical Society: Washington, DC, 1994; Vol. 537, pp 210−219.
(43) Calvert, J. M.; Calabrese, G. S.; Bohland, J. F.; Chen, M.-S.; Dressick, W. J.; Dulcey, C. S.; Georger, J. H.; Kosakowski, J.; Pavelcheck, E. K.; Rhee, K. W.; Shirey, L. M. *J. Vac. Sci. Technol. B* **1994**, *12*, 3884–3887.
(44) Dressick, W. J.; Dulcey, C. S.; Georger, J. H.; Calvert, J. M. *Chem. Mater.* **1993**, *5*, 148–150.
(45) Dressick, W. J.; Calvert, J. M. *Jpn. J. Appl. Phys., Part 1*, **1993**, *32* (12B), 5829–5839.
(46) Dressick, W. J.; Dulcey, C. S.; Calvert, J. M.; Georger, J. H.; Calabrese, G. S.; Thomas, M. E.; Stever, H. A. In *Advanced Metallization and Processing for Semiconductor Devices and Circuits II*; Katz, A., Murarka, S. P., Nissim, Y. I., Harper, J. M. E., Eds.; Materials Research Society: Warrendale, PA, 1992; Vol. 260, pp 659−664.
(47) Dulcey, C. S.; Georger, J. H.; Chen, M.-S.; McElvany, S. W.; O'Ferrall, C. E.; Benezra, V. I.; Calvert, J. M. *Langmuir* **1996**, *12*, 1638–1650.
(48) Friedli, A. C.; Roberts, R. D.; Dulcey, C. S.; Hsu, A. R.; McElvany, S. W.; Calvert, J. M. *Langmuir* **2004**, *20*, 4295–4298.
(49) Calvert, J. M.; Koloski, T. S.; Dressick, W. J.; Dulcey, C. S.; Peckerar, M. C.; Cerrina, F.; Taylor, J. W.; Suh, D. W.; Wood, O. R.; MacDowell, A. A.; D'Souza, R. *Opt. Eng.* **1993**, *32*, 2437–2445.
(50) Dressick, W. J.; Dulcey, C. S.; Brandow, S. L.; Witschi, H.; Neeley, P. F. *J. Vac. Sci. Technol. A* **1999**, *17*, 1432–1440.
(51) Yang, X. M.; Peters, R. D.; Kim, T. K.; Nealey, P. F.; Brandow, S. L.; Chen, M.-S.; Shirey, L. M.; Dressick, W. J. *Langmuir* **2001**, *17*, 228–233.
(52) Calvert, J. M.; Koloski, T. S.; Dressick, W. J.; Dulcey, C. S.; Peckerar, M. C.; Cerrina, F.; Taylor, J. W.; Suh, D. W.; Wood, O. R.; MacDowell, A. A.; D'Souza, R. *Proc. SPIE* **1993**, *1924*, 30–41.
(53) Marrian, C. R. K.; Perkins, F. K.; Brandow, S. L.; Koloski, T. S.; Dobisz, E. A.; Calvert, J. M. *Appl. Phys. Lett.* **1994**, *64*, 390–392.
(54) Perkins, F. K.; Dobisz, E. A.; Brandow, S. L.; Koloski, T. S.; Calvert, J. M.; Rhee, K. W.; Kosakowski, J. E.; Marrian, C. R. K. *J. Vac. Sci. Technol. B* **1994**, *12*, 3725–3730.
(55) Perkins, F. K.; Dobisz, E. A.; Marrian, C. R. K.; Brandow, S. L. *J. Vac. Sci. Technol. B* **1995**, *13*, 2841–2845.
(56) Perkins, F. K.; Dobisz, E. A.; Brandow, S. L.; Calvert, J. M.; Kosakowski, J. E.; Marrian, C. R. K. *Appl. Phys. Lett.* **1996**, *68*, 550–552.
(57) Brandow, S. L.; Calvert, J. M.; Snow, E. S.; Campbell, P. M. *J. Vac. Sci. Technol. A* **1997**, *15*, 1455–1459.
(58) Brandow, S. L.; Dressick, W. J.; Dulcey, C. S.; Koloski, T. S.; Shirey, L. M.; Schmidt, J.; Calvert, J. M. *J. Vac. Sci. Technol. B* **1997**, *15*, 1818–1824.
(59) Martin, B. D.; Brandow, S. L.; Dressick, W. J.; Schull, T. L. *Langmuir* **2000**, *16*, 9944–9946.
(60) Rhee, K. W.; Shirey, L. M.; Isaacson, P. I.; Komegay, C. F.; Dressick, W. J.; Chen, M.-S.; Brandow, S. L. *J. Vac. Sci. Technol. B* **2000**, *18*, 3569–3571.
(61) Brandow, S. L.; Schull, T. L.; Martin, B. D.; Guerin, D. C.; Dressick, W. J. *Chem.—Eur. J.* **2002**, *8*, 5363–5367.
(62) Ada, E. T.; Hanley, L.; Etchin, S.; Melngailis, J.; Dressick, W. J.; Chen, M.-S.; Calvert, J. M. *J. Vac. Sci. Technol. B* **1995**, *13*, 2189–2196.
(63) Brandow, S. L.; Chen, M.-S.; Dulcey, C. S.; Dressick, W. J. *Langmuir* **2008**, *24*, 3888–3896.
(64) Onclin, S.; Ravoo, B. J.; Reinhoudt, D. N. *Angew. Chem., Int. Ed.* **2005**, *44*, 6282–6304.
(65) Zharnikov, M.; Grunze, M. *J. Vac. Sci. Technol. B* **2002**, *20*, 1793–1807.
(66) Smith, R. K.; Lewis, P. A.; Weiss, P. S. *Prog. Surf. Sci.* **2004**, *75*, 1–68.
(67) Zhou, C.; Walker, A. V. *Langmuir* **2007**, *23*, 8876–8881.
(68) Artzi, R.; Daube, S. S.; Cohen, H.; Naaman, R. *Langmuir* **2003**, *19*, 7392–7398.
(69) Stewart, M. P.; Maya, F.; Kosynkin, D. V.; Dirk, S. M.; Stapleton, J. J.; McGuiness, C. L.; Allara, D. L.; Tour, J. M. *J. Am. Chem. Soc.* **2004**, *126*, 370–378.
(70) Mallory, G. O. In *Electroless Plating: Fundamentals and Applications*; Mallory, G. O., Hajdu, J. B., Eds.; American Electroplaters and Surface Finishers Society: Orlando, FL, 1990, pp 1−56.
(71) Demirel, M. C.; Cetinkaya, M.; Singh, A.; Dressick, W. J. *Adv. Mater.* **2007**, *19*, 4495–4499.
(72) Dinderman, M. A.; Dressick, W. J.; Kostelansky, C. N.; Price, R. R.; Qadri, S. B.; Schoen, P. E. *Chem. Mater.* **2006**, *18*, 4361–4368.
(73) Qadri, S. B.; Dinderman, M. A.; Dressick, W. J.; Schoen, P. E.; Lubitz, P.; He, J. H.; Tonucci, R. J.; Cross, J. *Appl. Phys. A: Mater. Sci. Process.* **2007**, *89*, 493–496.
(74) Koura, N.; Nagase, H.; Sato, A.; Kumakura, S.; Takeuchi, K.; Ui, K.; Tsuda, T.; Loong, C. K. *J. Electrochem. Soc.* **2008**, *155*, D155–D157.
(75) Ramasubramanian, M.; Popov, B. N.; White, R. E.; Chen, K. S. *J. Electrochem. Soc.* **1999**, *146*, 111–116.
(76) Chen, C.-H.; Chen, B.-H.; Hong, L. *Chem. Mater.* **2006**, *18*, 2959–2968.
(77) Petukhov, I. V. *Russ. J. Electrochem.* **2007**, *43*, 34–41.
(78) Petukhov, I. V. *Russ. J. Electrochem.* **2008**, *44*, 147–157.
(79) Valova, E.; Armyanov, S.; Dille, J.; van Ingelgem, Y.; Hubin, A.; Steenhaut, O. *J. Electrochem. Soc.* **2008**, *155*, D449–D458.
(80) Ohno, I. *Mater. Sci. Eng., A* **1991**, *146*, 33–49.
(81) Bindra, P.; Roldan, J. M.; Arbach, G. V. *IBM J. Res. Dev.* **1984**, *28*, 679–689.
(82) Zouhou, A.; Vergnes, H.; Duverneuil, P. *Microelectron. Eng.* **2001**, *56*, 177–180.
(83) Abrantes, L. M.; Correia, J. P. *J. Electrochem. Soc.* **1994**, *141*, 2356–2360.
(84) Homma, T.; Nakai, H.; Onishi, M.; Osaka, T. *J. Phys. Chem. B* **1999**, *103*, 1774–1778.
(85) Homma, T.; Komatsu, I.; Tamaki, A.; Nakai, H.; Osaka, T. *Electrochim. Acta* **2001**, *47*, 47–53.
(86) Nakai, H.; Homma, T.; Komatsu, I.; Osaka, T. *J. Phys. Chem. B* **2001**, *105*, 1701–1704.
(87) Homma, T.; Tamaki, A.; Nakai, H. *J. Electroanal. Chem.* **2003**, *559*, 131–136.
(88) Shimada, T.; Nakai, H.; Homma, T. *J. Electrochem. Soc.* **2007**, *154*, D273–D276.
(89) Yin, X.; Hong, L.; Chen, B.-H. *J. Phys. Chem. B* **2004**, *108*, 10919–10929.
(90) Chang, Y. L.; Ye, W. C.; Ma, C. L.; Wang, C. M. *J. Electrochem. Soc.* **2006**, *153*, C677–C682.
(91) Dimitrov, V.; Gorker, L. *Prog. React. Kinet. Mech.* **2006**, *31*, 45–58.
(92) Cohen, R. L.; West, K. W. *J. Electrochem. Soc.* **1973**, *120*, 502–508.
(93) Matijević, E.; Poskanzer, A. M.; Zuman, P. *Plat. Surf. Finish.* **1975**, *62*, 958–965.
(94) Koziol, G.; Bielinski, J. *Trans. Inst. Met. Finish.* **2003**, *81*, 110–113.
(95) Holderer, O.; Epicier, T.; Esnouf, C.; Fuchs, G. *J. Phys. Chem. B* **2003**, *107*, 1723–1726.
(96) Cohen, R. L.; West, K. W. *J. Electrochem. Soc.* **1972**, *119*, 433–438.
(97) Burrell, M. C.; Smith, G. A.; Chera, J. J. *Surf. Interface Anal.* **1988**, *11*, 160–164.
(98) Pierson, B.; Nebesny, K. W.; Fernando, Q.; Ogura, T. *Anal. Chem.* **1988**, *60*, 2661–2665.
(99) Froment, M.; Queau, E.; Martin, J. R.; Stremsdoerfer, G. *J. Electrochem. Soc.* **1995**, *142*, 3373–3377.
(100) Meek, R. L. *J. Electrochem. Soc.* **1975**, *122*, 1177–1185.
(101) O'Sullivan, E. J. M.; Horkans, J.; White, J. R.; Roldan, J. M. *IBM J. Res. Dev.* **1988**, *32*, 591–602.
(102) Huang, J.; Matsunaga, N.; Shimanoe, K.; Yamazoe, N.; Kunitake, T. *Chem. Mater.* **2005**, *17*, 3513–3518.
(103) Shukla, S.; Brinley, E.; Cho, H. J.; Seal, S. *Polymer* **2005**, *46*, 12130–12145.
(104) Shirahata, N.; Yokogawa, Y.; Kameyama, T.; Hozumi, A. *J. Vac. Sci. Technol. A* **2004**, *22*, 1734–1738.
(105) Gao, Y.; Koumoto, K. *Cryst. Growth Des.* **2005**, *5*, 1983–2017.
(106) Michel, B.; Bernard, A.; Bietsch, A.; Delamarche, E.; Geissler, M.; Juncker, D.; Kind, H.; Renault, J.-P.; Rothuizen, H.; Schmid, H.; Schmidt-Winkel, P.; Stutz, R.; Wolf, H. *IBM J. Res. Dev.* **2001**, *45*, 697–719.
(107) Geissler, M.; Kind, H.; Schmidt-Winkel, P.; Michel, B.; Delamarche, E. *Langmuir* **2003**, *19*, 6283–6296.
(108) Hsu, C.-H.; Yeh, M.-C.; Lo, K.-L.; Chen, L.-J. *Langmuir* **2007**, *23*, 12111–12118.

Downloaded by 194.44.31.30 on November 3, 2009 | http://pubs.acs.org
Publication Date (Web): January 12, 2009 | doi: 10.1021/am800121d

(109) Quist, A. P.; Pavlovic, E.; Oscarsson, S. *Anal. Bioanal. Chem.* **2005**, *381*, 591–600.
(110) Holtzman, A.; Richter, S. *J. Electrochem. Soc.* **2008**, *155*, D196–D202.
(111) Krivokapic, Z. U.S. Patent 6,623,803, 2003.
(112) Li, H.-W.; Muir, B. V. O.; Fichet, G.; Huck, W. T. S. *Langmuir* **2003**, *19*, 1963–1965.
(113) Zabetakis, D.; Dinderman, M.; Schoen, P. *Adv. Mater.* **2005**, *17*, 734–738.
(114) Khoperia, T. N.; Tabatadze, T. J.; Zedgenidze, T. I. *Electrochim. Acta* **1997**, *42*, 3049–3055.
(115) Viswanathan, B. *Curr. Sci.* **1993**, *65*, 537–543.
(116) Omura, Y.; Renbutsu, E.; Morimoto, M.; Saimoto, H.; Shigemasa, Y. *Polym. Adv. Technol.* **2003**, *14*, 35–39.
(117) Renbutsu, E.; Okabe, S.; Omura, Y.; Nakatsubo, F.; Minami, S.; Saimoto, H.; Shigemasa, Y. *Carbohydr. Polym.* **2007**, *69*, 697–706.
(118) Renbutsu, E.; Okabe, S.; Omura, Y.; Nakatsubo, F.; Minami, S.; Shigemasa, Y.; Saimoto, H. *Int. J. Biol. Macromol.* **2008**, *43*, 62–68.
(119) Schreiber, F. *Prog. Surf. Sci.* **2000**, *65*, 151–256.
(120) Mendes, P. A.; Preece, J. A. *Curr. Opin. Colloid Interface Sci.* **2004**, *9*, 236–248.
(121) Vargo, T. G., Jr.; Calvert, J. M.; Chen, M.-S. *Science* **1993**, *262*, 1711–1712.
(122) Kind, H.; Bittner, A. M.; Cavalleri, O.; Kern, K.; Greber, T. *J. Phys. Chem. B* **1998**, *102*, 7582–7589.
(123) Ivanova, V.; Baunach, T.; Kolb, D. M. *Electrochim. Acta* **2005**, *50*, 4283–4287.
(124) Boyen, H.-G.; Ziemann, P.; Wiedwald, U.; Ivanova, V.; Kolb, D. M.; Sakong, S.; Gross, A.; Romanyuk, A.; Büttner, M.; Oelhafen, P. *Nat. Mater.* **2006**, *5*, 394–399.
(125) Jacobs, J. W. M.; Rikken, J. M. G. *J. Electrochem. Soc.* **1988**, *135*, 2822–2827.
(126) Svendsen, L. G.; Osaka, T.; Sawai, H. *J. Electrochem. Soc.* **1983**, *130*, 2252–2255.
(127) Boily, J.-F.; Seward, T. M.; Charnock, J. M. *Geochim. Cosmochim. Acta* **2007**, *71*, 4834–4845.
(128) Good, N. E.; Winget, G. D.; Winter, W.; Connolly, T. N.; Izawa, S.; Singh, R. M. M. *Biochemistry* **1966**, *5*, 467–477.
(129) Kostelansky, C. N.; Pietron, J. J.; Chen, M.-S.; Dressick, W. J.; Swider-Lyons, K. E.; Ramaker, D. E.; Stroud, R. M.; Klug, C. A.; Zelakiewicz, B. S.; Schull, T. L. *J. Phys. Chem. B* **2006**, *110*, 21487–21496.
(130) Roland, B. *Microelectron. Eng.* **1991**, *13*, 11–18.
(131) Tipton, M.; Misium, G.; Garza, C.; Eguchi, M. *J. Vac. Sci. Technol. B* **1990**, *8*, 1740–1744.
(132) Misium, G. R.; Tipton, M.; Garza, C. M. *J. Vac. Sci. Technol. B* **1990**, *8*, 1749–1753.
(133) Coopmans, F.; Roland, B. *Solid State Technol.* **1987**, *30*, 93–99.
(134) Nalamasu, O.; Baiocchi, F. A.; Taylor, G. N. *Polymers in Microlithography*; ACS Sympoosium Series 412; American Chemical Society: Washington, DC, 1989; Vol. 412, pp 189—209.
(135) Katz, H. E.; Schilling, M. L.; Stein, S. M.; Houlihan, R. S.; Taylor, G. N. *Chem. Mater.* **1995**, *7*, 1534–1538.
(136) Taylor, G. N.; Hutton, R. S.; Stein, S. M.; Katz, H. E.; Schilling, M. L.; Putvinski, T. M. *Microelectron. Eng.* **1994**, *23*, 259–262.
(137) Schilling, M. L.; Katz, H. E.; Houlihan, F. M.; Stein, S. M.; Hutton, R. S.; Taylor, G. N. *J. Electrochem. Soc.* **1996**, *143*, 691–695.
(138) Schilling, M. L.; Katz, H. E.; Houlihan, F. M.; Kometani, J. M.; Stein, S. M.; Nalamasu, O. *Macromolecules* **1995**, *28*, 110–115.
(139) Calvert, J. M.; Chen, M.-S.; Dulcey, C. S.; Georger, J. H.; Peckerar, M. C.; Schnur, J. M.; Schoen, P. E. *J. Electrochem. Soc.* **1992**, *139*, 1677–1680.
(140) Calvert, J. M.; Georger, J. H.; Peckerar, M. C.; Pehrsson, P. E.; Schnur, J. M.; Schoen, P. E. *Thin Solid Films* **1992**, *210*, 359–363.
(141) Calvert, J. M.; Chen, M.-S.; Dulcey, C. S.; Georger, J. H.; Peckerar, M. C.; Schnur, J. M.; Schoen, P. E. *J. Vac. Sci. Technol. B* **1991**, *9*, 3447–3450.
(142) Calvert, J. M.; Dulcey, C. S.; Peckerar, M. C.; Schnur, J. M.; Georger, J. H.; Calabrese, G. S.; Sricharoenchaikit, P. *Solid State Technol.* **1991**, *34*, 77–82.
(143) Dulcey, C. S. Unpublished observations.
(144) Rivera, D.; Harris, J. M. *Langmuir* **2001**, *17*, 5527–5536.
(145) Shenderovich, I. G.; Buntkowsky, G.; Schreiber, A.; Gedat, E.; Sharif, S.; Albrecht, J.; Golubev, N. S.; Findenegg, G. H.; Limbach, H.-H. *J. Phys. Chem. B* **2003**, *107*, 11924–11939.
(146) Saito, N.; Hayashi, K.; Sugimura, H.; Takai, O. *J. Mater. Chem.* **2002**, *12*, 2684–2687.
(147) Hozumi, A.; Asakura, S.; Fuwa, A.; Shirahata, N.; Kameyama, T. *Langmuir* **2005**, *21*, 8234–8242.
(148) Sugimura, H.; Hong, L.; Lee, K.-H. *Jpn. J. Appl. Phys., Part 1* **2005**, *44* (7A), 5185–5187.
(149) Hartney, M. A.; Tarascon, R. G.; Novembre, A. E. *J. Vac. Sci. Technol. B* **1985**, *3*, 360–366.
(150) Brambley, D. R.; Jones, R. G.; Matsubayashi, Y.; Miller Tate, P. *J. Vac. Sci. Technol. B* **1990**, *8*, 1412–1417.
(151) Mixon, D. A.; Novembre, A. E.; Tai, W. W.; Jurgensen, C. W.; Frackoviak, J.; Trimble, L. E.; Kola, R. R.; Celler, G. K. *J. Vac. Sci. Technol. B* **1993**, *11*, 2834–2838.
(152) Koloski, T. S.; Dulcey, C. S.; Haralson, Q. J.; Calvert, J. M. *Langmuir* **1994**, *10*, 3122–3133.
(153) Reichmanis, E.; Nalamasu, O.; Houlihan, F. M.; Wallow, T. I.; Timko, A. G.; Cirelli, R.; Dabbagh, G.; Hutton, R. S.; Novembre, A. E.; Smith, B. W. *J. Vac. Sci. Technol. B* **1997**, *15*, 2528–2533.
(154) Doppelt, P.; Stelzle, M. *Microelectron. Eng.* **1997**, *33*, 15–23.
(155) Sun, S.; Montague, M.; Critchley, K.; Chen, M.-S.; Dressick, W. J.; Evans, S. D.; Leggett, G. J. *Nano Lett.* **2006**, *6*, 29–33.
(156) Maitlis, P. M. *The Organic Chemistry of Palladium. I. Metal Complexes*; Academic Press: New York, 1971.
(157) Brandow, S. L.; Calvert, J. M.; Dressick, W. J.; Dulcey, C. S. U.S. Patent 6,436,516, 2002.
(158) Merrifield, B. *Biosci. Rep.* **1985**, *5*, 353–376.
(159) Satoh, M.; Shirai, K.; Saitoh, H.; Yamauchi, T.; Tsubokawa, N. *J. Polym. Sci., Part A: Polym. Chem.* **2005**, *43*, 600–606.
(160) Frederich, N.; Nysten, B.; Muls, B.; Hofkens, J.; Habib Jiwan, J.-L.; Jonas, A. M. *Photochem. Photobiol. Sci.* **2008**, *7*, 460–466.
(161) Rathnayake, H. P.; Emrick, T. *Macromolecules* **2008**, *41*, 2969–2971.
(162) Malvadkar, N.; Park, S.; Urquidi-MacDonald, M.; Wang, H.; Demirel, M. C. *J. Power Sources* **2008**, *182*, 323–328.
(163) La, Y.-H.; Kim, H. J.; Maeng, I. S.; Jung, Y. J.; Park, J. W.; Kang, T.-H.; Kim, K.-J.; Ihm, K.; Kim, B. *Langmuir* **2002**, *18*, 301–303.
(164) La, Y.-H.; Jung, Y. J.; Kim, H. J.; Kang, T.-H.; Ihm, K.; Kim, K.-J.; Kim, B.; Park, J. W. *Langmuir* **2003**, *19*, 4390–4395.
(165) Hozumi, A.; Asakura, S.; Fuwa, A.; Shirahata, N. *J. Vac. Sci. Technol. A* **2005**, *23*, 1029–1033.
(166) Moon, S.; Chung, S.; Jeon, C.; Park, C.-Y.; Hwang, H.-N.; Hwang, C.-C.; Song, H.; Shin, H.-J. *Appl. Phys. Lett.* **2007**, *91*, 193104.
(167) Vanderputten, A. M. T.; Debakker, J. W. G. *J. Electrochem. Soc.* **1993**, *140*, 2229–2235.
(168) Ono, S.; Osaka, T.; Naitoh, K.; Nakagishi, Y. *J. Electrochem. Soc.* **1999**, *146*, 160–166.
(169) Lin, K.-L.; Wu, C.-H. *J. Electrochem. Soc.* **2003**, *150*, C273–C276.
(170) Long, D. P.; Dulcey, C. S. *J. Electrochem. Soc.* **2004**, *151*, G772–G782.
(171) Ito, H. *J. Photopolym. Sci. Technol.* **2008**, *21*, 475–491.
(172) Details of processing conditions for Figure 10. (All materials are Rohm & Haas, Shipley Inc. unless noted otherwise.) Part A: Note ref 36. Part B: O_2 plasma etch (2 min, 100 W RF, 1 Torr), EDA chemisorption (1% by volume of EDA(aq)/1 mM HOAc, 2 min puddle, spin-coat 15 s at 3000 rpm with an aqueous rinse and 15 s to dry), ~7-μm-thick AZ 4620 photoresist (Hoechst Inc.) deposition (spin-coated 30 s at 3000 rpm and baked 60 s at 115 °C), UV exposure (365—405 nm, ~380 mJ · cm^{-2}), 25% AZ140 (Hoechst Inc.) developer (120 s)/H_2O rinse, PD2 (2 min), NIPOSIT 468B EL Ni (10 min, 50 °C), AZ 4620 (Hoechst Inc.) resist remover (5 s), acetone rinse. Part C: Note ref 19. Part D: EUV processing, ~0.7-μm-thick planarizer deposition (S1400-26 photoresist spin-coated 30 s at 6000 rpm and thermally cross-linked 10 min at 210 °C), EDA chemisorption (1% by volume of EDA(aq)/1 mM HOAc, 20 min dip coating), SAL-601ER7 (diluted 1:3 with Thinner type A, spin-coated 30 s at 5000 rpm, and baked 30 min at 75 °C), EUV exposure (Schwartzchild camera, 13.4 nm, 8 mJ · cm^{-2}), postexposure bake (2 min, 115 °C), 0.27 N MF-312 development (6 min)/H_2O rinse, PD2 (2 min), 10% NIPOSIT 468 EL Ni (5 min, 25 °C), O_2 RIE (55 W RF, 10 mTorr, 45 nm · min^{-1}). Processing of the ~100-nm Ni gratings in Figure 10D (inset): Note ref 35.
(173) Osaka, T.; Takano, N.; Kurokawa, T.; Kaneko, T.; Ueno, K. *J. Electrochem. Soc.* **2002**, *149*, C573–C578.
(174) Osaka, T.; Takano, N.; Yokoshima, T. *Surf. Coat. Technol.* **2003**, *169*, 1–7.
(175) Osaka, T. *Chem. Rec.* **2004**, *4*, 346–362.

Downloaded by 194.44.31.30 on November 3, 2009 | http://pubs.acs.org
Publication Date (Web): January 12, 2009 | doi: 10.1021/am800121d

(176) Osaka, T.; Yoshino, M. *Electrochim. Acta* **2007**, *53*, 271–277.
(177) Yoshino, M.; Masuda, T.; Yokoshima, T.; Sasano, J.; Shacham-Diamand, Y.; Matsuda, I.; Osaka, T.; Hagiwara, Y.; Sato, I. *J. Electrochem. Soc.* **2007**, *154*, D122–D125.
(178) Kim, H. K.; Lee, J. P.; Park, C. R.; Kwak, H. T.; Sung, M. M. *J. Phys. Chem. B* **2003**, *107*, 4348–4351.
(179) Kluth, G. J.; Sung, M. M.; Maboudian, R. *Langmuir* **1997**, *13*, 3775–3780.
(180) Ganesan, P. G.; Cui, G.; Vijayamohanan, K.; Lane, M.; Ramanath, G. *J. Vac. Sci. Technol. B* **2005**, *23*, 327–331.
(181) Gandhi, D. D.; Lane, M.; Zhou, Y.; Singh, A. P.; Nayak, S.; Tisch, U.; Eizenberg, M.; Ramanath, G. *Nature* **2007**, *447*, 299–302.
(182) Krishnamoorthy, A.; Chanda, K.; Murarka, S. P.; Ramanath, G.; Ryan, J. G. *Appl. Phys. Lett.* **2001**, *78*, 2467–2469.
(183) Mikami, N.; Hata, N.; Kikkawa, T.; Machida, H. *Appl. Phys. Lett.* **2003**, *83*, 5181–5183.
(184) Ramanath, G.; Cui, G.; Ganesan, P. G.; Guo, X.; Ellis, A. V.; Stukowski, M.; Vijayamohanan, K.; Doppelt, P.; Lane, M. *Appl. Phys. Lett.* **2003**, *83*, 383–385.
(185) Gandhi, D. D.; Tisch, U.; Singh, B.; Eizenberg, M.; Ramanath, G. *Appl. Phys. Lett.* **2007**, *91*, 143503.
(186) Nakanishi, T.; Masuda, Y.; Koumoto, K. *Chem. Mater.* **2004**, *16*, 3484–3488.
(187) Saito, N.; Haneda, H.; Sekiguchi, T.; Ishigaki, T.; Koumoto, K. *J. Electrochem. Soc.* **2004**, *151*, H169–H173.
(188) Masuda, Y.; Kondo, M.; Koumoto, K. *Cryst. Growth Des.* **2009**, in press (DOI 10.1021/cg800856m).
(189) Wu, X. C.; Bittner, A. M.; Kern, K. *Langmuir* **2002**, *18*, 4984–4988.
(190) Knez, M.; Bittner, A. M.; Boes, F.; Wege, C.; Jeske, H.; Mai, E.; Kern, K. *Nano Lett.* **2003**, *3*, 1079–1082.
(191) Knez, M.; Sumser, M.; Bittner, A. M.; Wege, C.; Jeske, H.; Martin, T. P.; Kern, K. *Adv. Funct. Mater.* **2004**, *14*, 116–124.
(192) Yoshiki, H.; Hashimoto, K.; Fujishima, A. *J. Electrochem. Soc.* **1995**, *142*, 428–432.
(193) Gu, F.; Hashizume, M.; Okada, S.; Sasaki, Y.; Kikuchi, J.; Imori, T. *J. Ceram. Soc. Jpn.* **2008**, *116*, 400–405.
(194) Minamida, D.; Okada, S.; Hashizume, M.; Sasaki, Y.; Kikuchi, J.; Hosoito, N.; Imori, T. *J. Sol—Gel. Sci. Technol.* **2008**, *48*, 95–101.
(195) Charbonnier, M.; Romand, M.; Goepfert, Y.; Léonard, D.; Bessueille, F.; Bouadi, M. *Thin Solid Films* **2006**, *515*, 1623–1633.
(196) Xu, L. N.; Liao, J. H.; Huang, L.; Ou, D. L.; Zhou, K. C.; Zhang, H. Q.; Gu, N.; Liu, J. Z. *Chin. Chem. Lett.* **2002**, *13*, 687–688.
(197) Xu, L. N.; Liao, J. H.; Huang, L.; Gu, N.; Zhang, H. Q.; Liu, J. Z. *Appl. Surf. Sci.* **2003**, *211*, 184–188.
(198) Xu, L. N.; Zhou, K. C.; Xie, S. L.; Huang, L.; Gu, N. *Diffus. Defect Data, Pt. B* **2007**, *121—123*, 731–734.
(199) Ishii, D.; Yabu, H.; Shimomura, M. *Colloid Surf. A* **2008**, *313*, 590–594.
(200) Charbonnier, M.; Alami, M.; Romand, M. *J. Electrochem. Soc.* **1996**, *143*, 472–480.
(201) Charbonnier, M.; Romand, M.; Harry, E.; Alami, M. *J. Appl. Electrochem.* **2001**, *31*, 57–63.
(202) Charbonnier, M.; Romand, M. *Int. J. Adhes. Adhes.* **2003**, *23*, 277–285.
(203) Charbonnier, M.; Goepfert, Y.; Romand, M.; Leonard, D. *J. Adhes.* **2004**, *80*, 1103–1130.
(204) Wu, D.; Zhang, T.; Wang, W.-C.; Zhang, L.; Jin, R. *Polym. Adv. Technol.* **2008**, *19*, 335–341.
(205) Markowitz, M.; Baral, S.; Brandow, S. L.; Singh, A. *Thin Solid Films* **1993**, *224*, 242–247.
(206) Wang, T. C.; Chen, B.; Rubner, M. F.; Cohen, R. E. *Langmuir* **2001**, *17*, 6610–6615.
(207) Wang, T. C.; Rubner, M. F.; Cohen, R. E. *Chem. Mater.* **2003**, *15*, 299–304.
(208) Chen, Y.; Kang, E. T.; Neoh, K. G.; Huang, W. *Langmuir* **2001**, *17*, 7425–7432.
(209) Ma, Z. H.; Tan, K. L.; Alian, A. D.; Kang, E. T.; Neoh, K. G. *J. Vac. Sci. Technol. A* **2001**, *19*, 2471–2478.
(210) Yu, W. H.; Zhang, Y.; Kang, E. T.; Neoh, K. G.; Wu, S. Y.; Chow, Y. F. *J. Electrochem. Soc.* **2002**, *149*, C521–C528.
(211) Xu, D.; Kang, E. T.; Neoh, K. G.; Tay, A. A. O. *Langmuir* **2004**, *20*, 3324–3332.
(212) Li, L.; Yan, G.; Wu, J.; Yu, X.; Guo, Q.; Kang, E. *Appl. Surf. Sci.* **2008**, *254*, 7331–7335.
(213) Yu, Y. H.; Zhang, Y.; Kang, E. T.; Neoh, K. G.; Wu, S. Y.; Chow, Y. F. *J. Electrochem. Soc.* **2003**, *150*, F156–F163.
(214) Yu, W. H.; Kang, E. T.; Neoh, K. G. *Ind. Eng. Chem. Res.* **2004**, *43*, 5194–5202.
(215) Azzaroni, O.; Zheng, Z.; Yang, Z.; Huck, W. T. S. *Langmuir* **2006**, *22*, 6730–6733.
(216) Dai, W.; Wang, W. J. *Sens. Actuators, A* **2007**, *135*, 300–307.
(217) Miyoshi, K.; Aoki, Y.; Kunitake, T.; Fujikawa, S. *Langmuir* **2008**, *24*, 4205–4208.
(218) Zhu, P.; Masuda, Y.; Koumoto, K. *J. Mater. Chem.* **2004**, *14*, 976–981.
(219) Sawada, S.; Masuda, Y.; Zhu, P.; Koumoto, K. *Langmuir* **2006**, *22*, 332–337.
(220) Bicak, N.; Karagoz, B. *Surf. Coat. Technol.* **2008**, *202*, 1581–1587.
(221) Hsiao, Y.-S.; Whang, W.-T.; Wu, S.-C.; Chuang, K.-R. *Thin Solid Films* **2008**, *516*, 4258–4266.
(222) Charbonnier, M.; Romand, M.; Goepfert, Y. *Surf. Coat. Technol.* **2006**, *200*, 5028–5036.
(223) Charbonnier, M.; Romand, M.; Goepfert, Y.; Leonard, D.; Bouadi, M. *Surf. Coat. Technol.* **2006**, *200*, 5478–5486.
(224) Zangmeister, C. D.; van Zee, R. D. *Langmuir* **2003**, *19*, 8065–8068.
(225) Lu, P.; Walker, A. V. *Langmuir* **2007**, *23*, 12577–12582.
(226) Takano, N.; Hosoda, N.; Yamada, T.; Osaka, T. *J. Electrochem. Soc.* **1999**, *146*, 1407–1411.
(227) Chou, Y.-H.; Sung, Y.; Bai, C.-Y.; Ger, M.-D. *J. Electrochem. Soc.* **2008**, *155*, D551–D557.
(228) Ye, J.; Chen, Q. W.; Xiong, Y.; Chai, Y. S.; Chen, P. R. *Phys. Status Solidi A* **2008**, *205*, 1580–1584.
(229) Yamada, T.; Takano, N.; Yamada, K.; Yoshitomi, S.; Inoue, T.; Osaka, T. *Jpn. J. Appl. Phys., Part 1* **2001**, *40* (8), 4845–4853.
(230) Niwa, D.; Takano, N.; Yamada, T.; Osaka, T. *Electrochim. Acta* **2003**, *48*, 1295–1300.
(231) Niwa, D.; Homma, T.; Osaka, T. *J. Phys. Chem. B* **2004**, *108*, 9900–9904.
(232) Balachander, N.; Sukenik, C. N. *Langmuir* **1990**, *6*, 1621–1627.
(233) Fryxell, G. E.; Rieke, P. C.; Wood, L. L.; Engelhard, M. H.; Williford, R. E.; Graff, G. L.; Campbell, A. A.; Wiacek, R. J.; Lee, L.; Halverson, A. *Langmuir* **1996**, *12*, 5064–5075.
(234) Dulcey, C. S.; Koloski, T. S.; Dressick, W. J.; Calvert, J. M.; Peek, B. M. U.S. Patent 5,648,201, 1997.
(235) Higashi, J.; Nakayama, Y.; Marchant, R. E.; Matsuda, T. *Langmuir* **1999**, *15*, 2080–2088.
(236) Lex, A.; Trimmel, G.; Kern, W.; Stelzer, F. *J. Mol. Catal. A: Chem.* **2006**, *254*, 174–179.
(237) Lex, A.; Pacher, P.; Werzer, O.; Track, A.; Shen, Q.; Schennach, R.; Koller, G.; Hlawacek, G.; Zojer, E.; Resel, R.; Ramsey, M.; Teichert, C.; Kern, W.; Trimmel, G. *Chem. Mater.* **2008**, *20*, 2009–2015.
(238) Weinberger, M. R.; Langer, G.; Pogantsch, A.; Haase, A.; Zojer, E.; Kern, W. *Adv. Mater.* **2004**, *16*, 130–133.
(239) Nandivada, H.; Jiang, X.; Lahann, J. *Adv. Mater.* **2007**, *19*, 2197–2208.
(240) Bhatia, S. K.; Teixeira, J. L.; Anderson, M.; Shriver-Lake, L. C.; Calvert, J. M.; Georger, J. H.; Hickman, J. J.; Dulcey, C. S.; Schoen, P. E.; Ligler, F. S. *Anal. Biochem.* **1993**, *208*, 197–205.
(241) Liu, J.-F.; Zhang, L.-G.; Gu, N.; Ren, J.-Y.; Wu, Y.-P.; Lu, Z.-H.; Mao, P.-S.; Chen, D.-Y. *Thin Solid Films* **1998**, *327*, 176–179.
(242) Liu, L.; Engelhard, M. H.; Yan, M. *J. Am. Chem. Soc.* **2006**, *128*, 14067–14072.
(243) Jackson, R. L. *J. Electrochem. Soc.* **1990**, *137*, 95–101.
(244) Anderson, M. E.; Srinivasan, C.; Hohman, J. N.; Carter, E. M.; Horn, M. W.; Weiss, P. S. *Adv. Mater.* **2006**, *18*, 3258–3260.
(245) Tian, R.; Zhi, J. *Appl. Phys. Lett.* **2006**, *88*, 203102.
(246) Schönholzer, U. P.; Hummel, R.; Gauckler, L. J. *Adv. Mater.* **2000**, *12*, 1262–1263.
(247) Hang, Q.; Wang, Y.; Lieberman, M.; Bernstein, G. H. *Appl. Phys. Lett.* **2002**, *80*, 4220–4222.
(248) Harkness, B. R.; Rudolph, M.; Takeuchi, K. *Chem. Mater.* **2002**, *14*, 1448–1451.
(249) Schmidt, M. U.S. Patent 6,946,390, 2005.
(250) Porter, J. L. A.; Ribbe, A. E.; Buriak, J. M. *Nano Lett.* **2003**, *3*, 1043–1047.
(251) Bhuvana, T.; Kulkarni, G. U. *Bull. Mater. Sci.* **2008**, *31*, 201–206.
(252) Wada, Y. *Microelectron. J.* **1998**, *29*, 601–611.
(253) Cavallini, M.; Mei, P.; Biscarini, F.; García, R. *Appl. Phys. Lett.* **2003**, *83*, 5286–5288.

(254) Martínez, R. V.; Losilla, N. S.; Martinez, J.; Huttel, Y.; Garcia, R. *Nano Lett.* **2007**, *7*, 1846–1850.
(255) Chou, S. Y.; Zhuang, L.; Guo, L. *Appl. Phys. Lett.* **1999**, *75*, 1004–1006.
(256) Austin, M.; Chou, S. Y. *J. Vac. Sci. Technol. B* **2002**, *20*, 665–667.
(257) Colburn, M.; Grot, A.; Choi, B. J.; Amistoso, M.; Bailey, T.; Sreenivasan, S. V.; Ekerdt, J. G.; Willson, C. G. *J. Vac. Sci. Technol. B* **2001**, *19*, 2162–2172.
(258) Long, B. K.; Keitz, B. K.; Willson, C. G. *J. Mater. Chem.* **2007**, *17*, 3575–3580.
(259) Austin, M. D.; Ge, H.; Wu, W.; Li, M.; Yu, Z.; Wasserman, D.; Lyon, S. A.; Chou, S. Y. *Appl. Phys. Lett.* **2004**, *84*, 5299–5301.
(260) Krivokapic, Z. U.S. Patent 6,599,824, 2003.
(261) Maury, P.; Péter, M.; Mahalingam, V.; Reinhoudt, D. N.; Huskens, J. *Adv. Funct. Mater.* **2005**, *15*, 451–457.
(262) Kundu, S.; Liang, H. *Langmuir* **2008**, *24*, 9668–9674.
(263) Park, S. H.; Prior, M. W.; LaBean, T. H.; Finkelstein, G. *Appl. Phys. Lett.* **2006**, *89*, 033901.
(264) Chai, J.; Wang, D.; Fan, X.; Buriak, J. M. *Nat. Nanotechnol.* **2007**, *2*, 500–506.
(265) Natelson, D.; Willett, R. L.; West, K. W.; Pfeiffer, L. N. *Appl. Phys. Lett.* **2000**, *77*, 1991–1993.
(266) Zabet-Khosousi, A.; Dhirani, A.-A. *Chem. Rev.* **2008**, *108*, 4072–4124.
(267) Nilius, N.; Wallis, T. M.; Ho, W. *Science* **2002**, *297*, 1853–1856.
(268) Nilius, N.; Wallis, T. M.; Ho, W. *J. Phys. Chem. B* **2005**, *109*, 20657–20660.
(269) Thomas, P. J.; Kulkarni, G. U.; Rao, C. N. R. *J. Mater. Chem.* **2004**, *14*, 625–628.
(270) John, N. S.; Kulkarni, G. U. *J. Nanosci. Nanotechnol.* **2007**, *7*, 977–981.
(271) Li, Y.; Maynor, B. W.; Liu, J. *J. Am. Chem. Soc.* **2001**, *123*, 2105–2106.
(272) Maynor, B. W.; Li, Y.; Liu, J. *Langmuir* **2001**, *17*, 2575–2578.
(273) Basabe-Desmonts, L.; Wu, C.-C.; van der Werf, K. O.; Peter, M.; Bennink, M.; Otto, C.; Velders, A. H.; Reinhoudt, D. N.; Subramaniam, V.; Crego-Calama, M. *ChemPhysChem* **2008**, *9*, 1680–1687.

AM800121D

Downloaded by 194.44.31.30 on November 3, 2009 | http://pubs.acs.org
Publication Date (Web): January 12, 2009 | doi: 10.1021/am800121d